to Enza

each time I smile in my
life is simply because
she exists

Contents

Introduction

Quantitative theoretical predictions on a large number of interesting physical phenomena can be only made by relaying on numerical techniques. Highly non–linear partial differential equations as well as equations modeling many–body interacting systems are usually solved by replacing continuous space and time variables with a finite number of discrete lattice points. It becomes possible, in this way, to find solutions that however, because of the "granularity" of the space–time and the finite extension of the volume, come out to be approximate. In order for these solutions to have a required level of accuracy, upper limits on the sizes of the grid spacings and lower limits on the sizes of the finite volumes to be used in numerical calculations have to be met. It is usually not possible to fulfill such requirements at once because, for a given physical system, the smallest possible ratio between the grid spacing and the volume extension is limited by the available computing power. It often happens that the required space–time grid cannot be allocated on the computer memory or the time required to have a useful answer comes out to be unacceptably long, e.g. larger than a man life.

The problems discussed so far have been encountered by people working in different areas of physics and also in other fields of research. As a result of a joint effort, a wealth of theoretical techniques have been developed in order to extract phenomenological informations from the study of physical systems on unphysical volumes, the so called "finite volume techniques" (FVT). In this thesis three strong interacting physical systems are discussed that at first sight could appear to be uncorrelated. Actually, these subjects are glued together by the fact that in all of them it was necessary to use finite volume techniques in order to extract useful physical informations that otherwise would have been impossible to extract with the same level of accuracy.

The first physical system which will be considered is a heavy–light meson. Mesons are strong interacting particles and the study of their properties (masses, decay constants, decay rates, etc.) requires a non–perturbative formulation of the theory that can currently be achieved only by resorting to

the lattice regularization of Quantum Chromo Dynamics (QCD). In particular, heavy–light mesons represent a challenging system by the point of view of lattice QCD. The physics of a B meson, for example, is characterized by the presence of two largely separated energy scales, i.e. Λ_{QCD}, that sets the wavelengths of the light quark, and the b–quark mass. Dealing with these two scales in the most naive way would require a very large lattice. It should contain enough points to properly resolve the propagation of the heavy quark and at the same time make the light quark insensitive to finite volumes effects. A typical size would be $O(100^4)$ points, hardly affordable in terms of present day memory and CPU time. In ref. [1] it has been introduced a finite size method, called "Step Scaling Method" (SSM), devised to handle two–scale problems in lattice QCD and already applied to the study of typical heavy–light meson properties. Part I of this thesis is dedicated to a detailed presentation of the results of two lattice calculations that have been carried out in [2, 3] by making use of the SSM: the quenched lattice calculation of the b–quark mass and the B_s meson decay constant.

Part II is devoted to a discussion of the role played by the choice of boundary conditions in lattice calculations. As already said, in the formulation of quantum field theories on a lattice the introduction of a finite volume is unavoidable. As a consequence of the limited box size, spatial momenta come out to be quantized according to the choice of the boundary conditions and the momentum quantization represents a severe limitation in various phenomenological applications. In ref. [4] it has been pointed out that a particular choice of boundary conditions (BC), the so called θ-BC, is quite helpful in overcoming some of these difficulties. The application of this technique to the case of one and two particle states is discussed in chapters 4 and 5 respectively. In chapter 5 it is discussed how this choice of boundary conditions can be useful in attacking the long standing problem of the "$\Delta I = 1/2$ rule" in the non–leptonic weak decays such as in the case of $K \mapsto \pi\pi$.

Part I

Heavy Flavors

Chapter 1

Heavy flavor physics from finite volume calculations: the SSM

Lattice QCD evaluations of quantities characterized by two scales with a large hierarchy require in general a very high lattice resolution and a sizable total physical volume to correctly account the dynamics of the small distance scale and to dispose of the finite size effects related to the large distance scale. A concrete physical system in which this hierarchy problem appear and is hard to overcome is given by a heavy flavored hadron like for example the B meson.

Many different methods have been devised to study heavy flavor physics on the lattice. In almost all the cases quantitative predictions have been obtained by resorting to some approximation of the full theory, e.g. HQET on the lattice [5], lattice NRQCD [6], or QCD sum rules [7, 8]. A novel approach recently introduced solves the long standing problem of the non–perturbative renormalization of the static theory and of its matching to QCD [9, 10].

An alternative approach to lattice heavy flavor physics is the so called "Step Scaling Method" [1, 2, 3] or SSM in short. The main advantages of this method are that the entire computation is performed with the relativistic QCD Lagrangian and that the continuum limit can be taken, avoiding the unfeasible direct calculation. The idea behind SSM consists in using a QCD propagating b–quark on a small volume, calculating the finite volume effects on a given heavy–light observable and, finally, using the very mild dependence of these effects upon the heavy quark mass, to obtain a final result in a large volume. This chapter is dedicated to a detailed explanation of the SSM.

1.1 The "steps" of the SSM

On very general grounds, the method can be conveniently used in order to compute physical observables $\mathcal{O}(E_\ell, E_h)$ depending upon two largely separated energy scales E_ℓ and E_h ($E_\ell \ll E_h$), where direct simulation, without introducing big lattice artifacts, would require a very demanding computational effort. A SSM calculation is based on a very simple identity

$$\mathcal{O}(E_\ell, E_h, L_\infty) = \mathcal{O}(E_\ell, E_h, L_0)\ \frac{\mathcal{O}(E_\ell, E_h, 2L_0)}{\mathcal{O}(E_\ell, E_h, L_0)}\ \frac{\mathcal{O}(E_\ell, E_h, 4L_0)}{\mathcal{O}(E_\ell, E_h, 2L_0)}\ \ldots \quad (1.1)$$

stating that the value of the observable on the infinite volume is given by the product of its value on a finite volume L_0 with an infinite number of correcting factors called step scaling functions

$$\sigma_{\mathcal{O}}(E_\ell, E_h, L) = \frac{\mathcal{O}(E_\ell, E_h, 2L)}{\mathcal{O}(E_\ell, E_h, L)} \quad (1.2)$$

The step scaling functions are a measure of the error made when the value of O on the volume $2L$ is approximated with the corresponding value on the volume L. When the volume is sufficiently large this error becomes completely negligible and the step scaling functions cannot be distinguished by one within the numerical precision (δ_σ)

$$\sigma_{\mathcal{O}}(E_\ell, E_h, 2L_{max}) = 1 \pm \delta_\sigma \quad (1.3)$$

The previous equation has to be considered an implicit definition of the value L_{max}.

The main assumption under a SSM calculation is that the step scaling functions simplify in the region where $E_h \gg E_\ell$. In principle, a total decoupling of E_h would determine an absolute insensitivity to variations of this scale

$$\sigma_{\mathcal{O}}(E_\ell, E_h, L) \simeq \sigma_{\mathcal{O}}(E_\ell, L), \qquad E_h \gg E_\ell \quad (1.4)$$

In practice, E_h never completely decouples, but the mild residual dependence can be suitably parametrized. A typical situation is when the residual dependence upon E_h is linear in $1/E_h$ [1]. This assumption has to be checked numerically during the calculation and the whole procedure has to be aborted in case of a failure of this check.

The computation of the observable $\mathcal{O}$ proceeds according to the following lines. First, $\mathcal{O}$ is computed on a small finite volume L_0, where the high energy scale E_h can match its phenomenological value with the lattice cutoff much

larger than E_h. This computation is clearly unphysical, because the finiteness of the volume produces a distortion of the result, that cannot be compared with the experimental value. Second, the step scaling function is used in order to evolve this finite size measurement to a larger volume, according to eq. (1.1). Each step of the calculation can be extrapolated to the continuum limit. In the large volumes the step scaling functions are evaluated at the high energy scale E_h by extrapolation, relying on a suitable parametrization as will be better explained in the following section.

1.2 Properties of the step scaling functions

The step scaling functions defined in eq. (1.2) have many useful properties some of which can be derived by simple arguments.

By means of dimensional analysis it is easy to realize that since σ is a dimensionless quantity it can only depend upon dimensionless variables. The number of dimensionless independent quantities that can be obtained by combining L, E_ℓ and E_h is two. It is convenient to choose these variables to be LE_h and LE_ℓ

$$\sigma_{\mathcal{O}}(E_\ell, E_h, L) = \sigma_{\mathcal{O}}(LE_\ell, LE_h) \tag{1.5}$$

Indeed, the step scaling function can be rewritten as the value it would assume in the limit of very large volumes plus a "residual term" ($\gamma_{\mathcal{O}}$)

$$\sigma_{\mathcal{O}}(E_\ell, E_h, L) = 1 + \gamma_{\mathcal{O}}\left(\frac{1}{LE_\ell}, \frac{1}{LE_h}\right) \tag{1.6}$$

This term retains all the functional dependence of the step scaling function. In particular $\gamma_{\mathcal{O}}$, as it has been defined in the previous equation, vanishes when one (or both) of its arguments go to zero.

When the SSM has been introduced [1] the assumption of low sensitivity of the step scaling functions with respect to the high energy scale has been checked numerically in the case of the decay constants of heavy light mesons. Numerical data for the σ's at fixed volume had a residual linear dependence upon the inverse heavy quark mass (the high energy scale in this case). This leading linear behavior can be easily understood by considering a Taylor series expansion of the previous equation

$$\sigma_{\mathcal{O}}(E_\ell, E_h, L) = \left[1 + \gamma_{\mathcal{O}}\left(\frac{1}{LE_\ell}, 0\right)\right] + \frac{\gamma'_{\mathcal{O}}\left(\frac{1}{LE_\ell}, 0\right)}{LE_h} + \dots \tag{1.7}$$

The number of sizable terms in the previous expansion depend upon the particular observable and upon the required level of accuracy. When observables related to heavy flavor physics are considered, the dependence of the step scaling functions upon the inverse heavy quark masses can be predicted also by using HQET arguments (see sec. 1.4 below).

It should be noted that there are great advantages in considering the Taylor series expansion of the step scaling functions with respect to that of the observable. The first one is that the expansion parameter is the combination LE_h instead of a dimensional variable. The second one stays in the fact that one can reasonably expect some "cancellation" in the ratio between the observable calculated on different volumes making the derivative γ' smaller than the corresponding term arising in the expansion of $\mathcal{O}$. For these reasons it happens that in the case of the step scaling functions the high energy scale decouples from the low energy one on the contrary to what happens in the case of the observable itself. These points will be further clarified in the next two sections.

1.3 One scale problems, Step scaling functions and χ–PT

A deeper understanding of the properties of the step scaling functions can be obtained by studying a single scale problem. In this case the situation is simplified by the absence of the high energy scale and could be faced, for example, by a direct lattice calculation without recurring to finite volume techniques. Nevertheless, the simple identity of eq. (1.1) retains its validity also in the case of a light–light meson observable and can in principle be used to calculate the pion mass. In this case the step scaling function has the form

$$\sigma_{m_\pi}(m_\pi, L) = 1 + \gamma_{m_\pi}\left(\frac{1}{Lm_\pi}\right) \tag{1.8}$$

where again dimensional analysis it has been used to reduce the number of independent variables from two to one, i.e. Lm_π.

The fact that the step scaling functions do not depend separately upon the volume and upon the low energy scale ($m_\pi \simeq \Lambda_{QCD}$) can be checked in this case by using chiral perturbation theory [11, 12, 13, 14, 15, 16]. Indeed, chiral perturbation theory is well suited for the study of long–distance effects like those coming from the presence of a finite volume cutoff. Finite volume effects for the pion mass and decay constant have been derived in ref. [17]

in the case of θ–boundary conditions. It is a simple exercise to recast the results reported in this paper into the following form

$$\begin{aligned} \sigma_{m_\pi}(L, m_\pi) - 1 \qquad &\propto \qquad \frac{e^{-\frac{Lm_\pi}{2}}}{(Lm_\pi)^{\frac{3}{4}}} \\ \sigma_{f_\pi}(L, m_\pi) - 1 \qquad &\propto \qquad \frac{e^{-Lm_\pi}}{(Lm_\pi)^{\frac{3}{2}}} \end{aligned} \tag{1.9}$$

The previous relations refer to the choice of periodic boundary conditions for the pion interpolating operators. As can be seen, the step scaling functions do depend upon the combination Lm_π and approach one when this variable goes to infinity thus confirming the results obtained in the previous section by means of dimensional analysis.

1.4 Step scaling functions and HQET

When the step scaling method is used to calculate a particular observable that has a known expansion in terms of some of its arguments it is usually possible to derive additional useful properties of the step scaling functions. Obviously such kind of results will be valid only for the particular observable under consideration and have to be considered on a different ground with respect to the general properties of the σ's discussed so far. In this section it is considered the case of heavy–light mesons observables, the meson masses and decay constants. In these cases additional properties of the step scaling functions can be derived by using another effective theory of the QCD, the heavy quark effective theory (HQET). For good introductions to heavy quark effective theory and its applications see for example [18, 19].

In the infinite volume, heavy–light meson masses are predicted to have the following expansion in terms of the heavy quark mass

$$M_X(m_h, m_l) = m_h + \bar{\Lambda}(m_l) + \frac{\alpha_X(m_l)}{m_h} + \dots \tag{1.10}$$

where $X \in \{P, V\}$ refers to a pseudoscalar and a vector heavy–light meson respectively. Because of the matching coefficients [18, 19] $\alpha_X(m_l)$ can retain a small logarithmic dependence upon m_h that makes the HQET expansion different by a simple Taylor expansion. In the following this residual logarithmic dependence will not be considered because, although possible in principle, it is too hard to appreciate numerically the variations of the first order coefficients in the range of quark masses accessible to simulations of

lattice QCD, even by using the SSM. Assuming the contribution of the $1/m_h^2$ corrections to be negligible, at finite volume one has

$$M_X(m_h, m_l, L) = m_h + \bar{\Lambda}_X(m_l, L) + \frac{\alpha_X(m_l, L)}{m_h} \tag{1.11}$$

where $\bar{\Lambda}_X(m_l, L)$ depends upon the spin of the meson state because of the contamination of the excited states to the finite volume meson–meson correlations[1]. By using eq. (1.11) it is straightforward to obtain the HQET predictions for the step scaling functions of the heavy-light meson masses

$$\sigma_{M_X}(L, m_h, m_l) = 1 + \frac{\sigma^{(0)}_{M_X}(m_l, L)}{m_h} + \frac{\sigma^{(1)}_{M_X}(m_l, L)}{m_h^2} + \dots \tag{1.12}$$

This result requires some considerations. The first important thing to realize is that in the infinite heavy–quark mass limit the step scaling functions have to be exactly equal to one, $\sigma_{M_X}(L, m_l, m_h \to \infty) = 1$. This represents a strong constraint for the fits of the heavy–quark mass dependence of the step scaling functions.

The second observation concerns the number of terms to be considered in eq. (1.12). At order $O(1/m_h)$ one has

$$\sigma^{(0)}_{M_X}(m_l, L) = \bar{\Lambda}_X(m_l, 2L) - \bar{\Lambda}_X(m_l, L) \tag{1.13}$$

corresponding to the static approximation in eq. (1.11). By increasing the physical volume L, the difference between $\bar{\Lambda}_X(m_l, 2L)$ and $\bar{\Lambda}_X(m_l, L)$ decreases because the two quantities have to be equal in the infinite volume limit, making the heavy–quark mass expansion of the finite volume effects rapidly convergent. The same arguments apply to the coefficient $\sigma^{(1)}_X(m_l, L)$ that has to be considered when in the expansion of the meson masses, eq. (1.11), the order $O(1/m_h)$ is taken into account.

Similar results can be derived in the case of the decay constants. In the infinite volume the heavy-light mesons decay constants are predicted to have the following expression

$$f_X(m_l, m_h) = f^{(0)}(m_l) \left\{ 1 + \frac{G_X(m_l)}{m_h} + \dots \right\} \tag{1.14}$$

[1]Meson masses and decay constants are extracted on the lattice by studying the two–point functions of a meson interpolating operator. It is in general not possible on small volumes to isolate the ground state contributions to these correlations. This point will be discussed in detail in the next chapter (see section 2.4).

where again the residual logarithmic dependence has not been considered. The finite volume analogous of the previous expression is given by

$$f_X(m_l, m_h, L) = f_X^{(0)}(m_l, L) \left\{ 1 + \frac{G_X(m_l, L)}{m_h} + \ldots \right\} \tag{1.15}$$

where, as in the case of the finite volume binding energies, the so called finite volume "static" constants $f_X^{(0)}(L)$ acquire a dependence upon the spin content of the meson state because of the excited state contaminations of the meson–meson correlators. The step scaling functions are given by

$$\sigma_{f_X}(m_h, m_l, L) = \frac{f_X(m_l, 2L)}{f_X(m_l, L)} \left\{ 1 + \frac{G_X(m_l, 2L) - G_X(m_l, L)}{m_h} + \ldots \right\} \tag{1.16}$$

As in the case of the meson masses step scaling functions, the expansion is expected to be rapidly converging because $G_X(m_l, 2L)$ and $G_X(m_l, L)$ have to be equal on large enough volumes. The difference with respect to the case of the meson masses is that the static contribution in this case cannot be exactly predicted. For this reason, in order to reach the same level of accuracy in a SSM calculation of the meson masses and of the meson decay constants it is advisable, in the last case, to calculate independently the step scaling functions of the decay constants in the static approximation [20].

Chapter 2

Calculation of the heavy quark masses through the SSM

A precise calculation of the decay properties of the B mesons is required in order to reduce the theoretical uncertainties in the determination of the CP violating phase of the Cabibbo-Kobayashi-Maskawa (CKM) matrix but also to confront theoretical predictions against the experimental data produced at the B-factories with surprisingly high accuracy [21]. Crucial quantities in the so called Unitarity Triangle analysis [22, 23, 24] are, among the others, the B meson decay constant f_B and the b–quark mass.

This chapter is dedicated to the presentation of the results of a non–perturbative calculation of the b–quark mass through the application of the step scaling method. These results have been obtained in the quenched approximation of the QCD and by making use of the lattice regularization [2]. The strategy of the calculation consists in using the SSM to obtain the heavy–light and heavy–heavy meson masses as functions of the heavy quark masses chosen in the simulation. The b–quark mass is finally extracted by the comparison of the numerical results with the experimental results for the same quantities. As a byproduct of the calculation it has been also obtained a new determination of the c–quark mass.

The hierarchy problem discussed in the previous chapter does not arise in the case of charmed mesons because the number of points required to properly accommodate on the lattice a D meson, for example, is not prohibitive for current simulations of quenched QCD. Nevertheless charmed mesons spectrum have been calculated to cross check the results obtained by the SSM finite volume recursion against those of a direct calculation [25, 26]. The check has been successfully passed as will be explained below. In the case

of heavy–heavy mesons the hierarchy problem does even not arise but the heaviness of these hadrons makes the exponential decay of the meson correlation functions too fast and the ground state effective mass, at large time separations, cannot be disentangled from the numerical noise (at least on single precision architectures). As will be better explained in the following through the SSM it has been possible to handle also this problem.

2.1 Gauge action

Numerical calculations have been done within the quenched approximation of the QCD. It has been used the lattice regularization within the "Schrödinger Functional" (SF) formalism [27, 28]. The theory has been defined on a finite volume having physical extension T along the time direction and L along the spatial ones. All the simulated lattices had the topology $T = 2L$.

Gauge fields on the lattice are introduced by assigning to each point x and for each direction μ an $SU(3)$ matrix $U_\mu(x)$ representing the gauge connection between the points x and $x + a\hat{\mu}$ respectively. The boundary conditions satisfied by the $U_\mu(x)$ are chosen to be periodic along the spatial directions

$$U_\mu(x + L\hat{k}) = U_\mu(x) \tag{2.1}$$

and of the Dirichelet type along the time direction. In particular the links at $x_0 = 0$ and $x_0 = T$ have been fixed to be equal to the identity

$$U_\mu(x)|_{x_0=0} = 1 \qquad\qquad U_\mu(x)|_{x_0=T} = 1 \tag{2.2}$$

The gauge part of the action is chosen to be the usual Wilson plaquette action

$$S_G = -\frac{1}{\beta}\sum_p w(p)\,[1 - U(p)] + \delta S_{GB} \tag{2.3}$$

where $U(p)$ is the gauge connection along the plaquette p and the sum runs over all the oriented plaquettes on the lattice. The weight $w(p)$ is one for all the p except for the spatial ones attached at $x_0 = 0$ or $x_0 = T$ where it takes the value $1/2$. The term δS_{GB} is needed to implement $O(a)$ improvement within the SF formalism and is defined to be [27]

$$\delta S_{GB} = \frac{c_s - 1}{2g_0^2}\sum_{p_s}[1 - U(p_s)] + \frac{c_t - 1}{g_0^2}\sum_{p_t}[1 - U(p_t)] \tag{2.4}$$

the notations p_s and p_t mean that the sums run over all the spatial and time-like boundary plaquettes respectively. Since it has been chosen a vanishing

background field (2.2), spatial boundary plaquettes do not contribute to the action. Regarding c_t, the one loop result used in the simulations has been derived in [29].

2.2 Fermion action

Quark and antiquark fields carry Dirac and color indexes and are assigned to each lattice point. The boundary conditions, also in this case, have been chosen to be periodic in the space directions

$$\psi(x + L\hat{k}) = \psi(x) \qquad \overline{\psi}(x + L\hat{k}) = \overline{\psi}(x) \tag{2.5}$$

and fixed along the time direction. Only half of the Dirac components of the $\psi(x)$ are assigned at the two boundaries $x_0 = 0$ and $x_0 = T$

$$P_+ \, \psi(x)|_{x_0=0} = \zeta(x) \qquad P_- \, \psi(x)|_{x_0=T} = \zeta'(x) \tag{2.6}$$

In the previous conditions use have been made of the two projectors $P_\pm = (1 \pm \gamma_0)/2$. The corresponding boundary conditions for the antiquark fields are

$$\overline{\psi}(x)P_-\Big|_{x_0=0} = \overline{\zeta}(x) \qquad \overline{\psi}(x)P_+\Big|_{x_0=T} = \overline{\zeta}'(x) \tag{2.7}$$

Quark fields into the bulk ($0 < x_0 < T$) satisfy the $O(a)$ improved discrete version of the Dirac equation

$$(D_W + \delta D_{SW} + \delta D_B + m_0)\, \psi(x) = 0 \qquad 0 < x_0 < T \tag{2.8}$$

The leading Dirac operator have been fixed to be the standard Wilson operator D_W

$$D_W = \frac{1}{2}\left\{\gamma_\mu \left(\nabla_\mu + \nabla^\star_\mu\right) - a\nabla^\star_\mu\nabla_\mu\right\} \tag{2.9}$$

with the lattice covariant derivatives defined as

$$\nabla_\mu\psi(x) = \frac{1}{a}\left[U_\mu(x)\psi(x + a\hat{\mu}) - \psi(x)\right] \tag{2.10}$$

$$\nabla^\star_\mu\psi(x) = \frac{1}{a}\left[\psi(x) - U^{-1}_\mu(x - a\hat{\mu})\psi(x - a\hat{\mu})\right] \tag{2.11}$$

The remaining terms are needed to ameliorate the theory to order $O(a)$ [30, 31]. The improvement term δD_{SW} is proportional to the Pauli term and is given by

$$\delta D_{SW}\psi(x) = c_{SW}\frac{ia\sigma_{\mu\nu}\hat{F}_{\mu\nu}}{4}\psi(x) \tag{2.12}$$

where $\hat{F}_{\mu\nu}$ is a convenient lattice representation of the continuum gluon field strength tensor

$$\begin{aligned} \hat{F}_{\mu\nu}(x) &= \frac{1}{8a^2}\left\{Q_{\mu\nu}(x) - Q_{\nu\mu}(x)\right\} \\ Q_{\mu\nu}(x) &= U_\mu(x)U_\nu(x+a\hat{\mu})U_\mu^{-1}(x+a\hat{\nu})U_\nu^{-1}(x) \\ &+ U_\nu(x)U_\mu^{-1}(x-a\hat{\mu}+a\hat{\nu})U_\nu^{-1}(x-a\hat{\mu})U(x-a\hat{\mu},\mu) \\ &+ U_\mu^{-1}(x-a\hat{\mu})U_\nu^{-1}(x-a\hat{\mu}-a\hat{\nu})U_\mu(x-a\hat{\mu}-a\hat{\nu})U_\nu(x-a\hat{\nu}) \\ &+ U_\nu^{-1}(x-a\hat{\nu})U_\mu(x-a\hat{\nu})U_\nu(x+a\hat{\mu}-a\hat{\nu})U_\mu^{-1}(x) \end{aligned} \tag{2.13, 2.14}$$

The improvement boundary term is peculiar of the Schrödinger functional formalism and is given by [30, 31]

$$\begin{aligned} \delta D_B\psi(x) = \frac{\tilde{c}_t-1}{a} &\left\{\delta_{x_0,a}\left[\psi(x) - U_0^{-1}(x-a\hat{0})P_+\psi(x-a\hat{0})\right]\right. \\ &+ \left.\delta_{x_0,T-a}\left[\psi(x) - U_0(x)P_-\psi(x+a\hat{0})\right]\right\} \end{aligned} \tag{2.15}$$

2.3 Green functions

The mass of a meson can be calculated on the lattice by studying the decay of the two–point Green's function of an operator $\mathcal{O}(x)$ that has the same quantum numbers of the particle one is interested in. In this calculation have been calculated the masses of several heavy–light and heavy–heavy pseudoscalar and vector mesons made of quarks of masses covering the interesting physical range. The following operators have been considered

$$\begin{aligned} A_\mu(x) &= \overline{\psi}_i(x)\gamma_\mu\gamma_5\psi_j(x) \\ P(x) &= \overline{\psi}_i(x)\gamma_5\psi_j(x) \\ V_\mu(x) &= \overline{\psi}_i(x)\gamma_\mu\psi_j(x) \\ T_{\mu\nu}(x) &= \overline{\psi}_i(x)\gamma_\mu\gamma_\nu\psi_j(x) \end{aligned} \tag{2.16}$$

i.e. the axial current, the axial density, the local vector current and the tensor bilinear operator respectively (i and j are flavor indexes). The improvement of the axial and vector currents heave been implemented through the relations

$$\begin{aligned} A^I_\mu(x) &= A_\mu(x) + ac_A\ \tilde{\partial}_\mu P(x) \\ V^I_\mu(x) &= V_\mu(x) + ac_V\ \tilde{\partial}_\nu T_{\mu\nu}(x) \end{aligned} \tag{2.17}$$

where $\tilde{\partial}_\mu = (\partial_\mu + \partial^\star_\mu)/2$ and ∂_μ, $\partial^\star_\mu$ are given by

$$\begin{aligned} \partial_\mu \psi(x) &= \frac{1}{a}\left(\psi(x + a\hat{\mu}) - \psi(x)\right) \\ \partial^\star_\mu \psi(x) &= \frac{1}{a}\left(\psi(x) - \psi(x - a\hat{\mu})\right) \end{aligned} \tag{2.18}$$

For what concerns the improvement coefficients, c_A has been computed non perturbatively in ref. [32] while, in the case of c_V, non perturbative data have been used only at the values of the bare couplings where they exist [33] and perturbative results [34] have been used outside this range. The correlation functions used to compute pseudoscalar and vector meson masses have been defined by probing the previous operators with appropriate boundary sources

$$\begin{aligned} f^I_A(x_0) &= -\frac{a^6}{2}\sum_{\mathbf{y},\mathbf{z}} \langle \overline{\zeta}_j(\mathbf{y})\gamma_5\zeta_i(\mathbf{z}) A^I_0(x)\rangle \\ f_P(x_0) &= -\frac{a^6}{2}\sum_{\mathbf{y},\mathbf{z}} \langle \overline{\zeta}_j(\mathbf{y})\gamma_5\zeta_i(\mathbf{z}) P(x)\rangle \\ f^I_V(x_0) &= -\frac{a^6}{6}\sum_{\mathbf{y},\mathbf{z}} \langle \overline{\zeta}_j(\mathbf{y})\gamma_k\zeta_i(\mathbf{z}) V_k(x)\rangle \end{aligned} \tag{2.19}$$

where $\zeta_i(\mathbf{y})$ and $\overline{\zeta}_i(\mathbf{y})$ have been defined in sec. 2.3.

2.4 Excited states

In order to use the step scaling method in the calculation of the heavy meson spectrum it is necessary to define a procedure to measure meson masses on lattices of small physical volumes. Meson masses are usually extracted from the so called "effective mass"

$$aM_X(x_0) = \frac{1}{2}\ln\left[f_X(x_0 - a)/f_X(x_0 + a)\right] \tag{2.20}$$

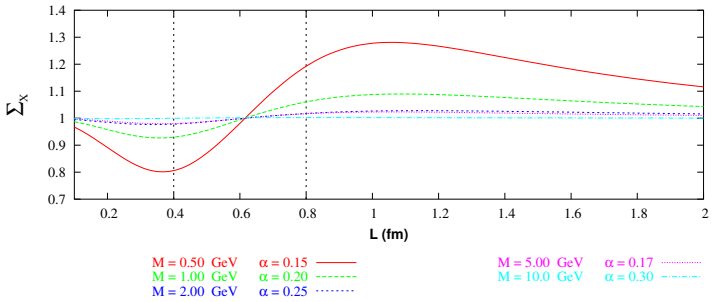

Figure 2.1: The figure shows the excited states finite size effect as predicted by a simplified qualitative model discussed in the text. The effective mass step scaling functions are plotted, at different values of the meson masses, as functions of the volume.

where f_X is one of the correlations defined in (2.19). On a physical volume, this quantity exhibits a plateau in the time region where the ground state dominates the correlation and no boundary effects are present. On a small volume the effective mass is affected by two different finite volume effects: the first one is due to the compression of the low energy wavelength (if present) and the second one comes from the presence of the excited states contribution to the correlation (no plateau). A good definition of the meson mass that suits the step scaling method is obtained by choosing the value of the effective mass at $x_0 = T/2$. All the lattices used in the present calculation have been chosen to have $T = 2L$. The step scaling technique (see eq.(1.1)) connects $x_0 = L_{min}$, where the meson mass has been defined on the smallest volume, with $x_0 = L_{max}$, where one expects to be free from both sources of finite volume effects.

The finite volume effects due to the excited states can be easily understood by means of a "two mass" model for the correlation

$$f_X(x_0, L) = A(L)\ e^{-M(L)x_0} + B(L)\ e^{-[M(L)+\delta M(L)]x_0} \tag{2.21}$$

Here $A(L)$ and $B(L)$ are coefficients, $M(L)$ is the meson mass and $\delta M(L)$ is the mass shift. All these quantities depend upon the physical extension of the volume L but, in order to isolate the effects due to the excited states, in the following M and δM will be considered as constants. In this simplified model the effective mass of eq. (2.20) takes the form

$$aM_X(x_0) = aM + \frac{1}{2}\ln\left\{\frac{1+\frac{B(L)}{A(L)}\ e^{-\delta M(x_0-a)}}{1+\frac{B(L)}{A(L)}\ e^{-\delta M(x_0+a)}}\right\} \tag{2.22}$$

As in numerical simulations, $x_0 = L$ is taken. The functional dependence upon the volume of the ratio $B(L)/A(L)$ can be inferred from the data on the meson decay constants given in [1, 3]. A parametrization that fits well the data is given by

$$A(L) = \alpha\left(1 + \frac{0.6}{L^2}\right) \qquad B(L) = -0.5 \tag{2.23}$$

In **Figure** [**2.1**] are shown the plots of the effective mass step scaling function, as derived from this model, defined by

$$\Sigma_X(L) = \frac{M_X(2L)}{M_X(L)} \tag{2.24}$$

as functions of the volume and at different values of the meson masses. At the volume $L = 0.4$ fm the step scaling functions are smaller than one while, the pattern is reversed at $L = 0.8$ fm. Independently from the volume, the heavier mesons are closer to unity than the lighter ones. The qualitative predictions of this simple model well reproduce the behavior of the numerically measured step scaling functions, shown in **Figure** [**2.3**] for $L = 0.4$ fm and in **Figure** [**2.6**] for $L = 0.8$ fm.

2.5 Quark mass definitions

Quark masses are fundamental parameters of the QCD Lagrangian. Their accurate knowledge is required in order to give quantitative predictions of fundamental processes. A direct experimental measurement of quark masses is not possible because of confinement, and their determination can only be inferred from a theoretical understanding of the hadron phenomenology. Furthermore, quark masses are subject to renormalization and their values depend upon the renormalization scheme and run with the renormalization scale. For each scheme it can be written the following renormalization group equation

$$\mu\frac{\partial\overline{m}_s}{\partial\mu} = \tau(\overline{g}_s)\overline{m}_s \qquad \overline{m}_s(\mu^0) = m_s^0 \tag{2.25}$$

The renormalized coupling constant $\overline{g}_s$ satisfies by its own the following equation

$$\mu\frac{\partial\overline{g}_s}{\partial\mu} = \beta(\overline{g}_s) \qquad \overline{g}_s(\mu^0) = g_s^0 \tag{2.26}$$

The QCD renormalized coupling gets vanishing for large values of the scale μ. In this regime the two functions $\beta(\overline{g}_s)$ and $\tau(\overline{g}_s)$ can be safely approximated

by their perturbative expansions

$$\beta(\overline{g}_s) = -\overline{g}_s^3 \sum_k b_k \overline{g}_s^k$$

$$\tau(\overline{g}_s) = -\overline{g}_s^2 \sum_k d_k \overline{g}_s^k \tag{2.27}$$

The coefficients of the previous expansions do in general depend upon the renormalization scheme. This is not the case of b_0 and b_1 and of d_0 and d_1 that are universal. The renormalization group equation (2.25) can be formally integrated with the following result

$$\overline{m}_s(\mu) = m^{RGI} (2b_0 \overline{g}^2)^{\frac{d_0}{2b_0}} e^{\int_0^{\overline{g}} dx \left[\frac{\tau(x)}{\beta(x)} - \frac{d_0}{b_0 x}\right]} \tag{2.28}$$

The previous equation implicitly defines the so called "renormalization group invariant" quark mass m^{RGI} that is a scheme and scale independent definition. In the following all the quark masses used in the calculation as well as the final results of the physical b and c quark masses will be expressed in this scheme.

The so–called bare current quark masses are defined through the lattice version of the PCAC relation

$$m_{ij}^{WI} = \frac{\tilde{\partial}_0 f_A(x_0) + a c_A \partial_0^\star \partial_0 f_P(x_0)}{2 f_P(x_0)} \tag{2.29}$$

These masses are connected to the renormalization group invariant quark masses through a renormalization factor which has been computed non–perturbatively in [35]:

$$m_{ij}^{RGI} = Z_M(g_0) \left[1 + (b_A - b_P) \frac{a m_i + a m_j}{2}\right] m_{ij}^{WI}(g_0) \tag{2.30}$$

where am_i is defined as

$$a m_i = \frac{1}{2}\left[\frac{1}{k_i} - \frac{1}{k_c}\right] \tag{2.31}$$

The combination $b_A - b_P$ of the improvement coefficients of the axial current and pseudoscalar density has been non–perturbatively computed in [36, 37]. The factor $Z_M(g_0)$ is known with very high precision in a range of inverse bare couplings that does not cover all the values of β used in the simulations. Nevertheless, the results reported in table (6) of ref. [35] have been used to parametrize $Z_M(g_0)$ in the enlarged range of β values $(5.9, 7.6)$. The RGI mass of a given quark is obtained from eq. (2.30) using the diagonal correlations

$$m_i^{RGI} = m_{ii}^{RGI} \tag{2.32}$$

From non–diagonal correlations in eq. (2.30) one obtains different $O(a)$ improved definitions of the RGI i–quark mass for different choices of the j–flavor:

$$m_{i_{\{j\}}}^{RGI} = 2m_{ij}^{RGI} - m_{jj}^{RGI} \tag{2.33}$$

All these definitions must have the same continuum limit because the dependence upon the j–flavor is only a lattice artifact. Further, in eq. (2.29) for each definition have been used either standard lattice time derivatives as well as improved ones [36, 37]. Another non–perturbative $O(a)$ improved definition of the RGI quark masses can be obtained starting from the bare quark mass

$$\hat{m}_i^{RGI} = Z_M(g_0)\ Z(g_0)\ [1 + b_m\ am_i]\ m_i \tag{2.34}$$

where the improvement coefficient b_m and the renormalization constant

$$Z(g_0) = \frac{Z_m Z_P}{Z_A} \tag{2.35}$$

have been non-perturbatively computed in ref. [36, 37].

Equations (2.32), (2.33) and (2.34) offer different possibilities to identify the valence quarks inside a given meson (fixed by the values of the bare quark masses). The procedure is well defined on small volumes because the RGI quark mass does not depend upon the scale and is defined in terms of local correlations that do not suffer finite volume effects. Each pair $\left(m_i^{RGI}, m_j^{RGI}\right)$ fixed a priori is matched, changing the values of the hopping parameters, by the different definitions of equations (2.32), (2.33) and (2.34), and leads to values of the corresponding meson mass differing by $O(a^2)$ lattice artifacts. Advantage have been taken of this plethora of definitions to constrain in a single fit the continuum extrapolations (see **Figure** [**2.2,2.4,2.7**]).

2.6 Lattice scale

In order to obtain physical predictions from a lattice QCD simulation, one has to spend as many "experimental" input as are the free parameters of the theory. One way to perform this task, in the case of a lattice extension large enough to safely account the dynamics of the light quarks, is to use the experimental inputs coming from the spectroscopy of the strange mesons. Another way to set the scale, widely used since its proposal [38], is based on the calculation of the force between static color sources; the physical input in this case is a length scale, $r_0 \simeq 0.5$ fm.

In [39] and then in [40] the ratio between the lattice spacing in physical units and the so called Sommer scale (a/r_0) has been computed for a range of $\beta \equiv 6/g_0^2$ going from $\beta_{min} = 5.7$ to $\beta_{max} = 6.92$ and a parametric description of $\ln(a/r_0)$ as a function of g_0^2 has been provided that describes the data with an accuracy better than 1 % in the whole range. In ref. [41] these results have been extended to larger values of β's by using a renormalization group analysis. In the following, physical results have been obtained by using $r_0 = 0.5$ fm.

2.7 Lattice simulations

As already explained in section 1.1 the step scaling method relies on the simple identity of eq. (1.1) that is rewritten here below in the case of the meson masses

$$\begin{aligned} M_X(m_\ell^{RGI}, m_h^{RGI}, L_{max}) = \quad & M_X(m_\ell^{RGI}, m_h^{RGI}, L_{max}) \times \\ & \times \frac{M_X(m_\ell^{RGI}, m_h^{RGI}, 2L_0)}{M_X(m_\ell^{RGI}, m_h^{RGI}, L_0)} \\ & \times \frac{M_X(m_\ell^{RGI}, m_h^{RGI}, 4L_0)}{M_X(m_\ell^{RGI}, m_h^{RGI}, 2L_0)} \end{aligned} \tag{2.36}$$

where $X \in \{P, V\}$ labels a pseudoscalar and a vector meson respectively. The physical extension of the small volume has been chosen in order to properly account the dynamics of quarks with masses in the region of the the physical b–quark; it has been fixed to be $L_0 = 0.4$ fm. Two evolution steps have been shown (see section 2.7.3) to be sufficient so that the recursion has been stopped at $L_{max} = 4L_0 = 1.6$ fm.

In the following the step scaling functions calculated at fixed lattice spacing will be referred to as Σ_X while the lower case symbol σ_X will be referring to the corresponding continuum results

$$\begin{aligned} \Sigma_X(m_\ell^{RGI}, m_h^{RGI}, L, a) &= \frac{M_X(m_\ell^{RGI}, m_h^{RGI}, 2L, a)}{M_X(m_\ell^{RGI}, m_h^{RGI}, L, a)} \\ \sigma_X(m_\ell^{RGI}, m_h^{RGI}, L) &= \lim_{a \mapsto 0} \Sigma_X(m_\ell^{RGI}, m_h^{RGI}, L, a) \end{aligned} \tag{2.37}$$

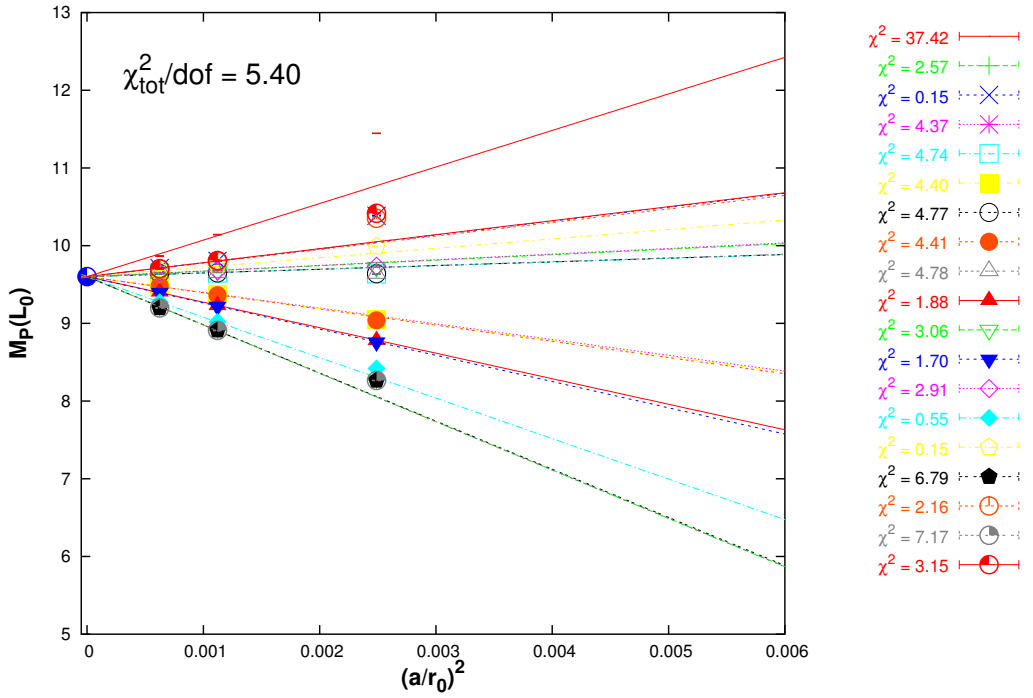

Figure 2.2: Continuum extrapolation on the small volume, L_0, of the mass $M_P(L_0)$ of the pseudoscalar heavy–heavy meson corresponding to the heavy quark of mass $m^{RGI} = 7.10$ GeV. The different values of the meson mass correspond to different definitions of the RGI quark masses given in equations (2.32), (2.33) and (2.34). Units are in GeV. Similar plots can be obtained, from the data reported in **Table** [**2.6,2.7,2.8**], for the other combinations of quark masses used in simulations, also in the case of $M_V(L_0)$.

2.7.1 Small volume

In order to have a continuum extrapolation of the numerical results, the volume $L_0 = 0.4$ fm has been simulated by three different discretization, 32×16^3, 48×24^3 and 64×32^3. By using the results reported in [26] two heavy quark masses have been chosen in such a way to interpolate the physical b–quark mass. In the renormalization group invariant (RGI) scheme these masses are 7.10 GeV and 6.60 GeV respectively. Two other heavy quarks have been simulated in order to interpolate the mass region where, using the results reported in [25, 26], one expects to find the physical c–quark, i.e. 1.70 GeV and 1.60 GeV respectively. An additional heavy quark has been simulated with mass 4.00 GeV. Three light quark have been simulated with

masses of 0.14 GeV, 0.10 GeV and 0.06 GeV. Using the accurate determination of the RGI strange quark mass given in [42] one of the simulated light quarks have been fixed to be the physical s. All the parameters of the three different simulations are summarized in **Table** [**2.3**]. The numerical results of the pseudoscalar and vector meson masses, M_P and M_V, are shown in **Table** [**2.6,2.7,2.8**] both for the heavy–heavy and for the heavy–light quark anti–quark pairs.

In order to obtain physical predictions from the simulated data on this finite volume the numerical results have been extrapolated to the continuum. As explained in section 2.5, different set of data have been obtained by using the different definitions of the RGI quark masses given in the equations (2.32), (2.33) and (2.34). The continuum results have then be obtained trough a combined fit of all the set of data, linear in $(a/r_0)^2$, as shown in **Figure** [**2.2**] in the case of the mass of the pseudoscalar heavy–heavy meson corresponding to the heavy quark of mass $m^{RGI} = 7.10$ GeV. A global $\chi^2/dof = 5.40$ is obtained to be compared with the χ^2s of each individual definition listed in the figure. The points at the largest lattice spacing are shown but have not been included in the fit. The errors included in the evaluation of the χ^2 are statistical only. These are calculated by a jackknife procedure, also in the case of the step scaling functions. The systematics due to the uncertainty on the lattice spacing has been estimated by repeating the fit using the different values of the scale allowed by the uncertainties quoted in [39, 40, 41] and considering the spread of the results. The same procedure has been used for the systematics due to the uncertainties on the renormalization constants. The resulting 2% percent for the renormalization constants and 1% percent for the scale have been summed in quadrature and added to the statistical errors at the end of the recursion.

2.7.2 First volume step

The finite volume effects on the quantities calculated at L_0, are measured by doubling the volume, $L_1 = 0.8$ fm. In order to have results in the continuum, also in the case of the step scaling functions three different discretizations of L_0 have been used, i.e 16×8^3, 24×12^3 and 32×16^3. The volume L_1 has been simulated starting from the discretizations of L_0, fixing the value of the bare coupling and doubling the number of lattice points in each direction. The simulated quark masses have been halved with respect to the masses simulated on the small volume in order to have the same order of discretization effects proportional to am (see the discussion of section 1.2). The set of parameters for the simulations of this evolution step is reported

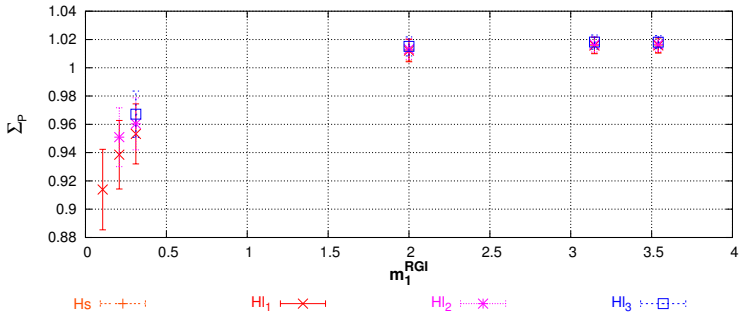

Figure 2.3: The figure shows the pseudoscalar step scaling functions Σ_P as functions of m_1^{RGI}, for the simulation of the first evolution step corresponding to $\beta = 6.963$. The different sets of data correspond to the values of m_2^{RGI}. As can be seen the step scaling functions approach a plateau for high values of m_1^{RGI}. Similar plots can be obtained using the data of **Table** [**2.9,2.10,2.11**] for the other values of the bare coupling and for the vector mesons step scaling functions Σ_V.

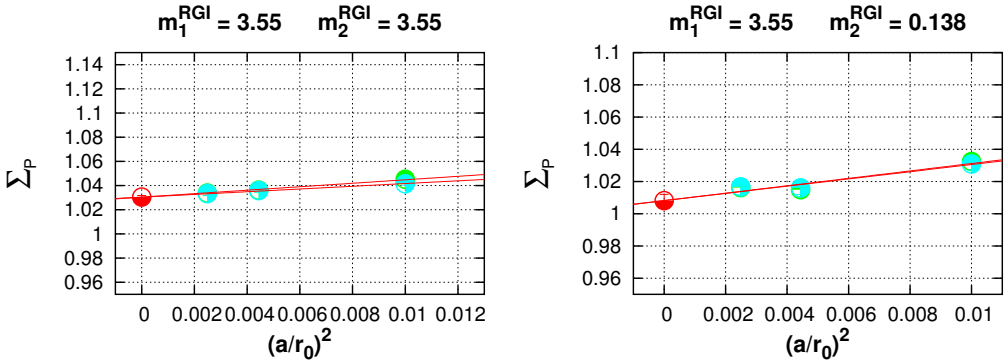

Figure 2.4: Continuum extrapolation on the first evolution step, $L_0 \mapsto L_1$, of the step scaling function, $\Sigma_P(L_0)$, of the pseudoscalar meson corresponding to the heavy quark of mass $m_1^{RGI} = 3.55$ GeV. The two sets of data are obtained using the two definitions of RGI quark masses of equations (2.32) and (2.34). Units are in GeV. Similar plots can be obtained, from the data reported in **Table** [**2.9,2.10,2.11**], for the other combinations of quark masses used in simulations, also in the case of $\Sigma_V(L_0)$.

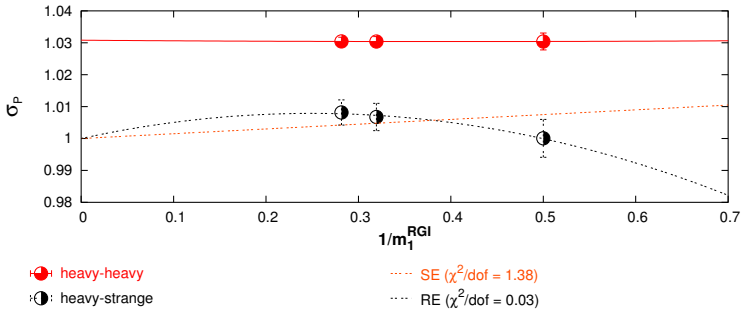

Figure 2.5: The figure shows the continuum extrapolated step scaling functions $\sigma_P(L_0)$ as functions of $1/m_1^{RGI}$. For the heavy–strange (Hs) set of data are shown both the linear (SE) and quadratic (RE) fits. Similar plots can be obtained using the data of **Table** [**2.9,2.10,2.11**] for the vector mesons step scaling functions $\sigma_V(L_0)$.

in **Table** [**2.4**] and the numerical results are given in **Table** [**2.9,2.10,2.11**].

The step scaling functions of the pseudoscalar mesons at $\beta = 6.963$ are plotted, at fixed m_2^{RGI}, as functions of m_1^{RGI} in **Figure** [**2.3**]. The value of the step scaling functions for the s quark are obtained trough linear interpolation. Both Σ_P and Σ_V are almost flat in a region of heavy quark masses starting around the charm mass. The hypothesis of low sensitivity upon the high–energy scale is thus *verified*. In **Figure** [**2.4**] are reported the results of the continuum extrapolation of the step scaling function, $\Sigma_P(L_0)$, of the pseudoscalar meson corresponding the heavy quark of mass $m_1^{RGI} = 3.55$ GeV. The residual heavy mass dependence of the continuum extrapolated step scaling functions is very mild, as shown in **Figure** [**2.5**] in the plot of σ_P as a function of the inverse quark mass. In the heavy–light case, as already discussed in section 1.4, the values of the step scaling functions at the values of the heavy–quark masses simulated on the small volume are extracted by interpolation between the numerical results and the theoretical point at $m_h^{RGI} \to \infty$ using both a linear fit (*SE*) and a quadratic fit (*RE*). In the heavy–heavy case the results are linearly extrapolated.

2.7.3 Second volume step

In order to have the results on a physical volume, $L_2 = 1.6$ fm, a second evolution step it has been required. This is done by computing the meson mass step scaling functions of eq. (2.37) at $L = L_1$, by the procedure outlined

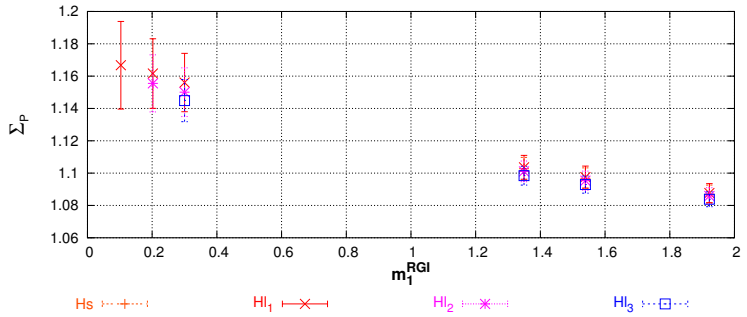

Figure 2.6: The figure shows the pseudoscalar step scaling functions Σ_P as functions of m_1^{RGI}, for the simulation of the second evolution step corresponding to $\beta = 6.420$. The different sets of data correspond to the values of m_2^{RGI}. Similar graphs can be obtained using the data of **Table** [**2.12,2.13,2.14**] for the other values of the bare coupling and for the vector mesons step scaling functions Σ_V.

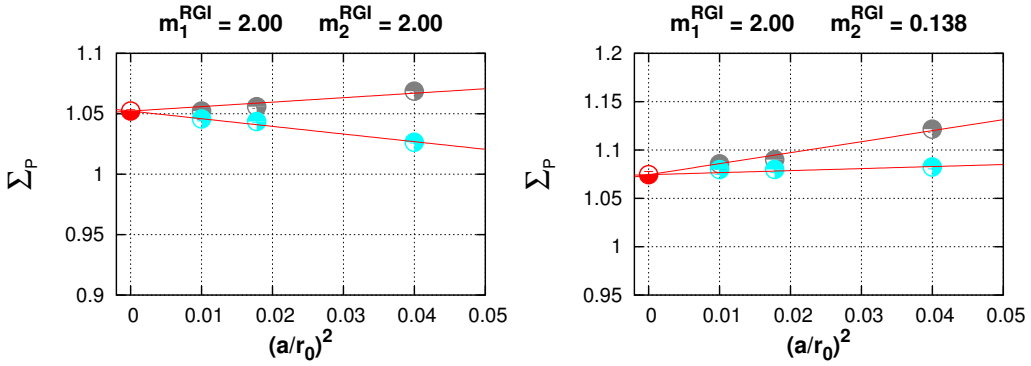

Figure 2.7: Continuum extrapolation on the second evolution step, $L_1 \mapsto L_2$, of the step scaling function, $\Sigma_P(L_1)$, of the pseudoscalar meson corresponding to the heavy quark of mass $m_1^{RGI} = 2.00$ GeV. The two sets of data are obtained using the two definitions of RGI quark masses of equations (2.32) and (2.34). Units are in GeV. Similar plots can be obtained, from the data reported in **Table** [**2.12,2.13,2.14**], for the other combinations of quark masses used in simulations, also in the case of $\Sigma_V(L_1)$.

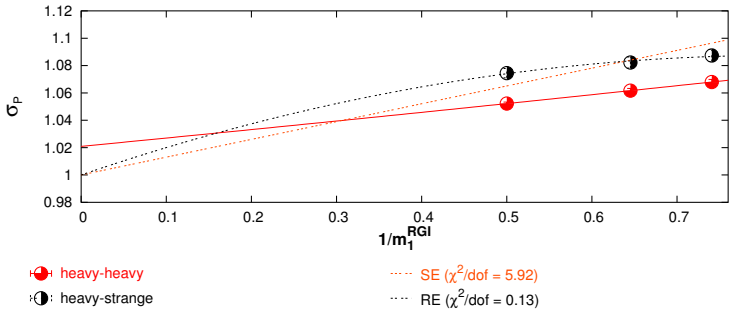

Figure 2.8: The figure shows the continuum extrapolated step scaling functions $\sigma_P(L_1)$ as functions of $1/m_1^{RGI}$. For the heavy–strange (Hs) set of data are shown both the linear (SE) and quadratic (RE) fits. Similar plots can be obtained using the data of **Table** [**2.12,2.13,2.14**] for the vector mesons step scaling functions $\sigma_V(L_1)$.

in the previous section. The parameters of the simulations are given in **Table** [**2.5**] and the results are in **Table** [**2.12,2.13,2.14**].

Also in this case, the values of the simulated quark masses have been halved with respect to the previous step, owing to the lower values of the simulation cutoffs. In **Figure** [**2.6**] are shown the pseudoscalar step scaling functions at $\beta = 6.420$ and in **Figure** [**2.8**] the residual heavy–quark mass dependence with the *SE* and *RE* fits. **Figure** [**2.7**] shows the continuum extrapolation of the step scaling function, $\Sigma_P(L_1)$, of the pseudoscalar meson corresponding to the heavy quark of mass $m_1^{RGI} = 2.00$ GeV. The contributions of the excited states, predicted from the simple model of eq. (2.24) and present in our numerical data, should disappear in a third evolution step. A check supporting this hypothesis is that on the larger volumes used in the simulation of this evolution step, i.e. L_2 at $\beta = 6.420$ and $\beta = 6.211$, the values of the meson masses defined at $x_0 = T/2$ coincide, within the errors, with the values coming from a "single mass" fit to the correlations.

2.8 Physical results

In this section the results of the small volume are combined with the results of the step scaling functions to obtain, according to eq. (1.1), the physical numbers. In **Table** [**2.1**] are shown the pseudoscalar and vector meson masses corresponding to the heavy quarks simulated on the small volume and, in the heavy–light case, to strange and up light quarks. The results corresponding to

m_h^{RGI}	State	M_P	M_V
7.10	$\bar{h}h$	10.11(22)	10.12(22)
	$\bar{h}s$	5.48(13)	5.52(13)
	$\bar{h}u$	5.40(16)	5.44(16)
6.60	$\bar{h}h$	9.49(21)	9.50(21)
	$\bar{h}s$	5.18(12)	5.22(12)
	$\bar{h}u$	5.10(15)	5.14(15)
4.00	$\bar{h}h$	6.18(14)	6.20(14)
	$\bar{h}s$	3.55(8)	3.62(8)
	$\bar{h}u$	3.46(10)	3.53(11)
1.70	$\bar{h}h$	3.15(7)	3.21(7)
	$\bar{h}s$	1.97(5)	2.09(5)
	$\bar{h}u$	1.88(6)	2.00(6)
1.60	$\bar{h}h$	3.01(7)	3.07(7)
	$\bar{h}s$	1.90(5)	2.01(5)
	$\bar{h}u$	1.80(5)	1.93(6)

Table 2.1: Meson masses in the infinite volume limit. Units are in GeV.

State	m_h^{RGI}	
	from P	from V
$\bar{b}b$	6.44(14)	6.57(14)
$\bar{b}s$	6.91(16)	6.93(16)
$\bar{b}u$	6.90(20)	6.91(20)
$\bar{c}c$	1.603(35)	1.642(36)
$\bar{c}s$	1.692(38)	1.741(39)
$\bar{c}u$	1.690(50)	1.712(51)

Table 2.2: Determinations of the heavy quark masses from the heavy–heavy and from the heavy–light states. The errors include our estimate of the systematics. Units are in GeV.

the up quark have been obtained by extrapolating the continuum data in the large volume from masses around the strange region. In **Figure** [**2.9**] we show the extrapolation for the pseudoscalar meson corresponding to $m_h^{RGI} = 7.1$ GeV. Having simulated three light quark on the largest volume we have fitted the results linearly without trying complicated functional forms requiring more than two parameters. Comparing these results with the experimental determinations of the same quantities [26] have been obtained different determinations of the b–quark mass, depending upon the physical state used as experimental input. The results are summarized in **Table** [**2.2**].

Within the quenched approximation, the determinations of the quark masses coming from the heavy–heavy or from the heavy–light spectrum in

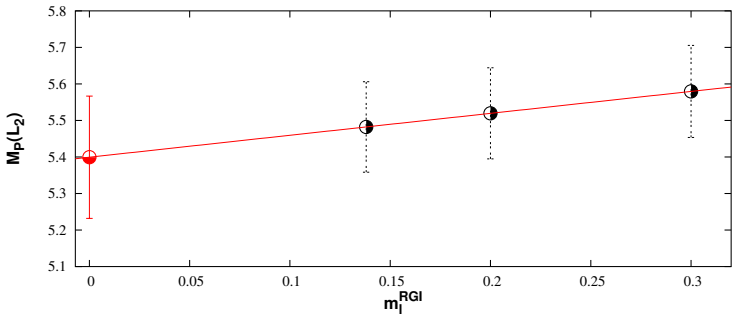

Figure 2.9: Chiral extrapolation of the continuum results for the pseudoscalar meson corresponding to $m_h^{RGI} = 7.1$. Units are in GeV.

principle differ because the theory does not account for the fermion loops. In the present calculation have been obtained two determinations that are marginally compatible within the errors and that might suggest the need for a tiny unquenching effect. The good agreement between the determinations of the quark masses coming from the heavy–up and heavy–strange sets of data is an implicit check of the chiral extrapolations. Of course the heavy–strange and the heavy–heavy case are not extrapolated at all and therefore only these results are used to determine the heavy–quark masses. The numbers below, i.e. the final results of the calculation, are obtained by averaging the four results in the first two rows of the two sets of **Table** [**2.2**] for the heavy-heavy and the heavy-strange cases and by keeping the typical error of a single case:

$$m_b^{RGI} = 6.73(16)\ \text{GeV} \qquad m_b^{\overline{MS}}(m_b^{\overline{MS}}) = 4.33(10)\ \text{GeV} \tag{2.38}$$

for the b–quark and

$$m_c^{RGI} = 1.681(36)\ \text{GeV} \qquad m_c^{\overline{MS}}(m_c^{\overline{MS}}) = 1.319(28)\ \text{GeV} \tag{2.39}$$

for the charm. The latter results compare favorably with the results of the direct computations [25, 26].

As already explained in section 2.7.1, the error estimate includes both the *statistical* error from the Monte Carlo simulation as well as the *systematic* error coming from the uncertainty on the lattice spacing corresponding at a given β value and to the uncertainty on the renormalization constants in eqs (2.30) and (2.34). The final errors on the continuum quantities, of the order of 2% percent for the renormalization constants and of about 1% percent for the scale, are summed in quadrature and added to the statistical errors. The evolution to the $\overline{MS}$ scheme has been done using four–loop renormalization group equations [43, 44, 45].

β	L/a	k_c	k	m^{RGI} (GeV)
6.963	16	0.134827(6)	0.120081	7.14(8)
			0.120988	6.63(7)
			0.126050	4.024(44)
			0.131082	1.696(19)
			0.131314	1.591(18)
			0.134526	0.1381(30)
			0.134614	0.0978(28)
			0.134702	0.0574(28)
7.300	24	0.134235(3)	0.124176	7.11(8)
			0.124844	6.61(20)
			0.128440	4.018(44)
			0.131800	1.695(19)
			0.131950	1.592(18)
			0.134041	0.1374(27)
			0.134098	0.0971(24)
			0.134155	0.0567(24)
7.548	32	0.133838(2)	0.126352	7.10(8)
			0.126866	6.60(7)
			0.129585	4.016(44)
			0.132053	1.698(19)
			0.132162	1.595(18)
			0.133690	0.1422(27)
			0.133732	0.1021(25)
			0.133773	0.0618(23)

Table 2.3: Simulation parameters at $L_0 = 0.4$ fm. The RGI quark masses are obtained using eq. (2.32).

β	L_0/a	k_c	k	m^{RGI} (GeV)
6.420	8	0.135703(9)	0.120674	3.543(39)
			0.122220	3.114(34)
			0.126937	1.927(21)
			0.134304	0.3007(36)
			0.134770	0.2003(28)
			0.135221	0.1028(21)
6.737	12	0.135235(5)	0.1249	3.542(39)
			0.1260	3.136(34)
			0.1293	1.979(22)
			0.1343	0.3127(38)
			0.1346	0.2090(28)
			0.1349	0.1080(21)
6.963	16	0.134832(4)	0.127074	3.549(39)
			0.127913	3.153(35)
			0.130409	2.003(22)
			0.134145	0.3134(38)
			0.134369	0.2112(28)
			0.134593	0.1086(20)

Table 2.4: Simulation parameters for the first evolution step $L_0 \to L_1 = 0.8$ fm. The RGI quark masses are obtained using eq. (2.32).

β	L_1/a	k_c	k	m^{RGI} (GeV)
5.960	8	0.13490(4)	0.118128	2.012(22)
			0.121012	1.551(17)
			0.122513	1.337(15)
			0.131457	0.3154(36)
			0.132335	0.2322(28)
			0.133226	0.1466(44)
6.211	12	0.135831(8)	0.124090	1.984(22)
			0.126198	1.584(17)
			0.127280	1.389(15)
			0.133574	0.3493(39)
			0.134177	0.2550(29)
			0.134786	0.1510(19)
6.420	16	0.135734(5)	0.126996	1.933(21)
			0.128646	1.547(17)
			0.129487	1.355(14)
			0.134318	0.3016(34)
			0.134775	0.2038(24)
			0.135235	0.1055(15)

Table 2.5: Simulation parameters for the first evolution step $L_1 \to L_2 = 1.6$ fm. The RGI quark masses are obtained using eq. (2.32).

β	m_1^{RGI}	m_2^{RGI}	M_P	M_V
	7.14(8)	7.14(8)	8.295(5)	8.318(5)
		6.63(7)	8.092(5)	8.116(6)
		4.024(44)	6.898(6)	6.924(6)
		1.696(19)	5.590(7)	5.622(7)
		1.591(18)	5.527(7)	5.559(8)
		0.1381(30)	4.646(9)	4.691(10)
		0.0978(28)	4.622(10)	4.668(10)
		0.0574(28)	4.597(10)	4.645(10)
	6.63(7)	6.63(7)	7.888(5)	7.913(6)
		4.024(44)	6.693(6)	6.721(6)
		1.696(19)	5.384(7)	5.417(7)
		1.591(18)	5.320(7)	5.354(8)
		0.1381(30)	4.438(9)	4.485(10)
		0.0978(28)	4.414(10)	4.462(10)
		0.0574(28)	4.390(10)	4.440(10)
6.963	4.024(44)	4.024(44)	5.491(6)	5.524(7)
		1.696(19)	4.170(7)	4.215(8)
		1.591(18)	4.106(7)	4.152(8)
		0.1381(30)	3.207(10)	3.278(11)
		0.0978(28)	3.183(10)	3.255(11)
		0.0574(28)	3.158(10)	3.232(11)
	1.696(19)	1.696(19)	2.826(8)	2.898(9)
		1.591(18)	2.760(8)	2.835(9)
		0.1381(30)	1.816(10)	1.952(12)
		0.0978(28)	1.790(10)	1.928(12)
		0.0574(28)	1.763(10)	1.905(12)
	1.591(18)	1.591(18)	2.694(8)	2.771(9)
		0.1381(30)	1.746(10)	1.888(12)
		0.0978(28)	1.719(10)	1.864(12)
		0.0574(28)	1.692(10)	1.840(12)

Table 2.6: Values of the pseudoscalar, M_P, and vector, M_V, meson masses resulting from the simulations on the smallest volume $L_0 = 0.4$ fm at $\beta = 6.963$. Units are in GeV.

β	m_1^{RGI}	m_2^{RGI}	M_P	M_V
	7.11(8)	7.11(8)	8.920(6)	8.944(7)
		6.61(20)	8.678(6)	8.702(7)
		4.018(44)	7.310(7)	7.336(8)
		1.695(19)	5.926(9)	5.957(10)
		1.592(18)	5.862(9)	5.893(10)
		0.1374(27)	4.987(13)	5.031(14)
		0.0971(24)	4.964(14)	5.009(14)
		0.0567(24)	4.942(14)	4.987(15)
	6.61(20)	6.61(20)	8.435(6)	8.459(7)
		4.018(44)	7.066(7)	7.093(8)
		1.695(19)	5.680(9)	5.713(10)
		1.592(18)	5.616(9)	5.649(10)
		0.1374(27)	4.739(13)	4.786(14)
		0.0971(24)	4.717(14)	4.764(15)
		0.0567(24)	4.694(14)	4.742(15)
7.300	4.018(44)	4.018(44)	5.689(8)	5.722(9)
		1.695(19)	4.291(10)	4.336(11)
		1.592(18)	4.226(10)	4.272(11)
		0.1374(27)	3.334(14)	3.404(15)
		0.0971(24)	3.310(14)	3.381(15)
		0.0567(24)	3.287(14)	3.359(16)
	1.695(19)	1.695(19)	2.869(11)	2.942(13)
		1.592(18)	2.803(11)	2.878(13)
		0.1374(27)	1.864(14)	1.999(17)
		0.0971(24)	1.838(14)	1.976(17)
		0.0567(24)	1.812(15)	1.953(17)
	1.592(18)	1.592(18)	2.736(11)	2.813(13)
		0.1374(27)	1.793(14)	1.934(17)
		0.0971(24)	1.767(14)	1.911(17)
		0.0567(24)	1.741(15)	1.888(18)

Table 2.7: Values of the pseudoscalar, M_P, and vector, M_V, meson masses resulting from the simulations on the smallest volume $L_0 = 0.4$ fm at $\beta = 7.300$. Units are in GeV.

β	m_1^{RGI}	m_2^{RGI}	M_P	M_V
	7.10(8)	7.10(8)	9.203(7)	9.225(8)
		6.60(7)	8.939(7)	8.960(8)
		4.016(44)	7.480(8)	7.503(9)
		1.698(19)	6.060(10)	6.088(10)
		1.595(18)	5.996(10)	6.025(11)
		0.1422(27)	5.115(14)	5.157(15)
		0.1021(25)	5.093(14)	5.135(15)
		0.0618(23)	5.070(15)	5.113(15)
	6.60(7)	6.60(7)	8.674(7)	8.696(8)
		4.016(44)	7.214(8)	7.238(9)
		1.698(19)	5.792(10)	5.822(11)
		1.595(18)	5.728(10)	5.759(12)
		0.1422(27)	4.846(14)	4.891(15)
		0.1021(25)	4.823(14)	4.869(15)
		0.0618(23)	4.801(15)	4.847(15)
7.548	4.016(44)	4.016(44)	5.746(9)	5.776(10)
		1.698(19)	4.314(10)	4.356(11)
		1.595(18)	4.249(10)	4.292(12)
		0.1422(27)	3.352(15)	3.420(15)
		0.1021(25)	3.328(15)	3.398(16)
		0.0618(23)	3.305(15)	3.377(16)
	1.698(19)	1.698(19)	2.860(11)	2.930(13)
		1.595(18)	2.794(11)	2.866(13)
		0.1422(27)	1.852(15)	1.988(17)
		0.1021(25)	1.827(15)	1.966(17)
		0.0618(23)	1.801(16)	1.944(18)
	1.595(18)	1.595(18)	2.727(12)	2.802(13)
		0.1422(27)	1.781(15)	1.924(17)
		0.1021(25)	1.756(15)	1.901(18)
		0.0618(23)	1.730(16)	1.879(18)

Table 2.8: Values of the pseudoscalar, M_P, and vector, M_V, meson masses resulting from the simulations on the smallest volume $L_0 = 0.4$ fm at $\beta = 7.548$. Units are in GeV.

β	m_1^{RGI}	m_2^{RGI}	Σ_P	Σ_V
	0.1028(21)	0.1028(21)	0.996(28)	0.826(21)
		0.2003(28)	1.010(23)	0.848(19)
		0.3007(36)	1.017(20)	0.869(17)
		1.927(21)	1.034(7)	0.998(8)
		3.114(34)	1.032(5)	1.013(6)
		3.543(39)	1.031(5)	1.015(5)
	0.2003(28)	0.2003(28)	1.016(20)	0.867(17)
		0.3007(36)	1.020(18)	0.885(15)
		1.927(21)	1.036(7)	1.003(7)
		3.114(34)	1.034(5)	1.015(5)
		3.543(39)	1.037(5)	1.018(5)
6.420	0.3007(36)	0.3007(36)	1.022(16)	0.901(14)
		1.927(21)	1.038(6)	1.007(7)
		3.114(34)	1.036(5)	1.019(5)
		3.543(39)	1.0349(46)	1.0205(47)
	1.927(21)	1.927(21)	1.0520(34)	1.0425(37)
		3.114(34)	1.0493(27)	1.0438(29)
		3.543(39)	1.0479(25)	1.0433(27)
	3.114(34)	3.114(34)	1.0471(21)	1.0440(23)
		3.543(39)	1.0460(20)	1.0433(22)
	3.543(39)	3.543(39)	1.0449(19)	1.0427(20)

Table 2.9: Values of the step scaling functions for the pseudoscalar, Σ_P, and vector, Σ_V, meson masses resulting from the simulation at $\beta = 6.420$ of the first evolution step $L_0 \to L_1$. Units are in GeV.

β	m_1^{RGI}	m_2^{RGI}	Σ_P	Σ_V
	0.1080(21)	0.1080(21)	0.907(25)	0.789(19)
		0.2090(28)	0.935(21)	0.810(17)
		0.3127(38)	0.951(19)	0.830(16)
		1.979(22)	1.009(7)	0.976(7)
		3.136(34)	1.014(5)	0.995(5)
		3.542(39)	1.014(5)	0.998(5)
	0.2090(28)	0.2090(28)	0.950(18)	0.828(16)
		0.3127(38)	0.960(16)	0.846(14)
		1.979(22)	1.011(6)	0.980(7)
		3.136(34)	1.0155(47)	0.998(5)
		3.542(39)	1.0158(43)	1.0009(46)
6.737	0.3127(38)	0.3127(38)	0.967(14)	0.862(13)
		1.979(22)	1.014(6)	0.985(6)
		3.136(34)	1.0176(44)	1.0013(47)
		3.542(39)	1.0178(40)	1.0039(43)
	1.979(22)	1.979(22)	1.0376(30)	1.0279(33)
		3.136(34)	1.0375(23)	1.0317(25)
		3.542(39)	1.0367(21)	1.0317(23)
	3.136(34)	3.136(34)	1.0372(18)	1.0338(19)
		3.542(39)	1.0365(16)	1.0336(18)
	3.542(39)	3.542(39)	1.0358(15)	1.0333(17)

Table 2.10: Values of the step scaling functions for the pseudoscalar, Σ_P, and vector, Σ_V, meson masses resulting from the simulation at $\beta = 6.737$ of the first evolution step $L_0 \to L_1$. Units are in GeV.

β	m_1^{RGI}	m_2^{RGI}	Σ_P	Σ_V
	0.1086(20)	0.1086(20)	0.914(28)	0.783(24)
		0.2112(28)	0.939(24)	0.807(21)
		0.3134(38)	0.953(21)	0.830(19)
		2.003(22)	1.012(8)	0.981(8)
		3.153(35)	1.016(6)	0.999(6)
		3.549(39)	1.016(5)	1.002(6)
	0.2112(28)	0.2112(28)	0.951(21)	0.828(19)
		0.3134(38)	0.960(18)	0.847(17)
		2.003(22)	1.013(7)	0.984(8)
		3.153(35)	1.017(5)	1.001(6)
		3.549(39)	1.017(5)	1.003(5)
6.963	0.3134(38)	0.3134(38)	0.967(16)	0.864(16)
		2.003(22)	1.015(7)	0.989(7)
		3.153(35)	1.018(5)	1.004(5)
		3.549(39)	1.0181(46)	1.006(5)
	2.003(22)	2.003(22)	1.0365(35)	1.0281(39)
		3.153(35)	1.0357(27)	1.0309(30)
		3.549(39)	1.0348(25)	1.0307(28)
	3.153(35)	3.153(35)	1.0349(21)	1.0321(23)
		3.549(39)	1.0341(20)	1.0317(22)
	3.549(39)	3.549(39)	1.0333(19)	1.0313(20)

Table 2.11: Values of the step scaling functions for the pseudoscalar, Σ_P, and vector, Σ_V, meson masses resulting from the simulation at $\beta = 6.963$ of the first evolution step $L_0 \to L_1$. Units are in GeV.

β	m_1^{RGI}	m_2^{RGI}	Σ_P	Σ_V
	0.1466(44)	0.1466(44)	1.269(13)	1.308(15)
		0.2322(28)	1.244(11)	1.286(12)
		0.3154(36)	1.226(9)	1.267(10)
		1.337(15)	1.1406(40)	1.1636(45)
		1.551(17)	1.1332(37)	1.1539(42)
		2.012(22)	1.1214(32)	1.1383(36)
	0.2322(28)	0.2322(28)	1.224(9)	1.266(10)
		0.3154(36)	1.209(8)	1.249(9)
		1.337(15)	1.1337(35)	1.1557(40)
		1.551(17)	1.1268(32)	1.1467(37)
		2.012(22)	1.1158(29)	1.1322(32)
5.960	0.3154(36)	0.3154(36)	1.196(7)	1.235(8)
		1.337(15)	1.1278(32)	1.1489(37)
		1.551(17)	1.1213(30)	1.1405(34)
		2.012(22)	1.1110(27)	1.1269(30)
	1.337(15)	1.337(15)	1.0894(19)	1.029(21)
		1.551(17)	1.0853(18)	1.0978(20)
		2.012(22)	1.0785(16)	1.0895(17)
	1.551(17)	1.551(17)	1.0814(17)	1.0931(18)
		2.012(22)	1.0749(15)	1.0852(16)
	2.012(22)	2.012(22)	1.0689(13)	1.0782(14)

Table 2.12: Values of the step scaling functions for the pseudoscalar, Σ_P, and vector, Σ_V, meson masses resulting from the simulation at $\beta = 5.960$ of the second evolution step $L_1 \to L_2$. Units are in GeV.

β	m_1^{RGI}	m_2^{RGI}	Σ_P	Σ_V
	0.1510(19)	0.1510(19)	1.156(14)	1.255(18)
		0.2550(29)	1.151(11)	1.235(15)
		0.3493(39)	1.146(10)	1.219(12)
		1.389(15)	1.1035(46)	1.131(6)
		1.584(17)	1.1098(42)	1.123(5)
		1.984(22)	1.0899(37)	1.1095(44)
	0.2550(29)	0.2550(29)	1.147(10)	1.218(12)
		0.3493(39)	1.142(8)	1.204(10)
		1.389(15)	1.1010(40)	1.1258(48)
		1.584(17)	1.0961(37)	1.1181(44)
		1.984(22)	1.0879(33)	1.1056(39)
6.211	0.3493(39)	0.3493(39)	1.138(7)	1.193(9)
		1.389(15)	1.0983(37)	1.1210(44)
		1.584(17)	1.0936(34)	1.1137(40)
		1.984(22)	1.0857(30)	1.1020(35)
	1.389(15)	1.389(15)	1.0727(20)	1.0842(24)
		1.584(17)	1.0695(19)	1.0799(22)
		1.984(22)	1.0640(17)	1.0728(20)
	1.584(17)	1.584(17)	1.0664(18)	1.0759(21)
		1.984(22)	1.0611(16)	1.0692(18)
	1.984(22)	1.984(22)	1.0564(14)	1.0633(16)

Table 2.13: Values of the step scaling functions for the pseudoscalar, Σ_P, and vector, Σ_V, meson masses resulting from the simulation at $\beta = 6.211$ of the second evolution step $L_1 \to L_2$. Units are in GeV.

β	m_1^{RGI}	m_2^{RGI}	Σ_P	Σ_V
	0.1055(15)	0.1055(15)	1.167(27)	1.259(35)
		0.2038(24)	1.162(22)	1.235(27)
		0.3016(34)	1.156(18)	1.218(22)
		1.355(14)	1.104(7)	1.125(9)
		1.547(17)	1.098(7)	1.117(8)
		1.933(21)	1.088(6)	1.103(7)
	0.2038(24)	0.2038(24)	1.155(18)	1.217(21)
		0.3016(34)	1.150(15)	1.203(18)
		1.355(14)	1.101(6)	1.121(8)
		1.547(17)	1.095(6)	1.113(7)
		1.933(21)	1.086(5)	1.000(6)
6.420	0.3016(34)	0.3016(34)	1.144(13)	1.192(16)
		1.355(14)	1.098(6)	1.118(7)
		1.547(17)	1.093(5)	1.110(6)
		1.933(21)	1.0839(46)	1.098(5)
	1.355(14)	1.355(14)	1.0711(31)	1.0821(37)
		1.547(17)	1.0676(29)	1.0777(34)
		1.933(21)	1.0617(25)	1.0702(30)
	1.547(17)	1.547(17)	1.0643(27)	1.0735(31)
		1.933(21)	1.0587(24)	1.0665(27)
	1.933(21)	1.933(21)	1.0538(21)	1.0604(24)

Table 2.14: Values of the step scaling functions for the pseudoscalar, Σ_P, and vector, Σ_V, meson masses resulting from the simulation at $\beta = 6.420$ of the second evolution step $L_1 \to L_2$. Units are in GeV.

Chapter 3

Calculation of heavy–light mesons decay constants through the SSM

In the previous chapter the step scaling method has been used to calculate heavy meson masses and to extract the quenched value of the b–quark mass. The method has been also applied to the calculation of the B_s meson decay constant [3] and this chapter is dedicated to a presentation of these results. As an outcome of the calculation it has been also determined the decay constant of the D_s meson. In this way it has been possible to compare the SSM result against that of a direct calculation with a successful outcome. The calculation of the b–quark mass and that of the B_s meson decay constant have been carried on in parallel on the same set of data. For this reason this chapter inherits all the notations explained in the previous one and is mainly focused on the numerical results.

3.1 Definition of the observable

Meson decay constants on a finite volume are defined through the correlations introduced in section 2.3. In particular, the decay constant of a heavy–light pseudoscalar meson is given by

$$f_{h\ell} = \frac{2}{\sqrt{L^3 M_P(T/2)}} \frac{f_A^R(T/2)}{\sqrt{f_1}} \tag{3.1}$$

The correlation $f_A^R(x_0)$ is defined as (see eq. (2.17))

$$\begin{aligned} f_A^R(x_0) &= -\frac{a^6}{2}\sum_{\mathbf{y},\mathbf{z}}\langle\overline{\zeta}_j(\mathbf{y})\gamma_5\zeta_i(\mathbf{z})A_0^R(x)\rangle \\ A_\mu^R(x_0) &= Z_A\ (1+b_A\frac{am_i+am_j}{2})\ A_\mu^I(x_0) \end{aligned} \tag{3.2}$$

where am_i is the bare quark mass of the i quark and Z_A is the axial current renormalization constant that has been computed non perturbatively in [46]. For the improvement coefficient b_A have been used the perturbative results quoted in [34] (at the values of the bare coupling, $\beta \simeq 7.0$, used in the numerical simulations the one–loop contribution to b_A differs from the tree–level of 10%). The pseudoscalar meson mass $M_P(x_0)$ has been defined in eq. (2.20) while f_1 is the boundary–to–boundary correlation needed in order to cancel, in the ratio, the renormalization constants of the boundary quark fields:

$$f_1 = -\frac{a^{12}}{3L^6}\sum_{\mathbf{y},\mathbf{z},\mathbf{u},\mathbf{w}}\ \langle\ \overline{\zeta}_j(\mathbf{y})\gamma_5\zeta_i(\mathbf{z})\ \overline{\zeta'}_i(\mathbf{u})\gamma_5\zeta'_j(\mathbf{w})\ \rangle \tag{3.3}$$

It is important to realize that the choice of defining the decay constant in the middle of the lattice, $x_0 = T/2$, does not introduces other length scales than L into the calculation (see the analogous discussion in the case of the meson masses, section 2.4). Indeed the topology of the simulated finite volumes is such that $T = 2L$ and the step scaling technique (see eq.(1.1)) connects $x_0 = L_{min}$, where the decay constant has been defined on the smallest volume, with $x_0 = L_{max}$, where one expects to be free from finite volume effects.

3.2 Lattice Simulations

As already mentioned, the results of the heavy–light mesons decay constants have been extracted from the same simulations and from the same numerical data produced in the calculation of the quark masses. The small volume have been fixed to be $L_0 = 0.4$ fm and the recursion has been stopped after two steps, at the volume $L_{max} = 1.6$ fm. The SSM identity in the case of the decay constants is simply given by

$$f_{h\ell}(L_{max}) = f_{h\ell}(L_0)\ \frac{f_{h\ell}(2L_0)}{f_{h\ell}(L_0)}\ \frac{f_{h\ell}(4L_0)}{f_{h\ell}(2L_0)} \tag{3.4}$$

In the following, the step scaling functions at finite lattice spacing will be referred to as Σ wile the continuum one will be called σ

$$\Sigma_{h\ell}(L,a) = \frac{f_{h\ell}(2L,a)}{f_{h\ell}(L,a)}$$

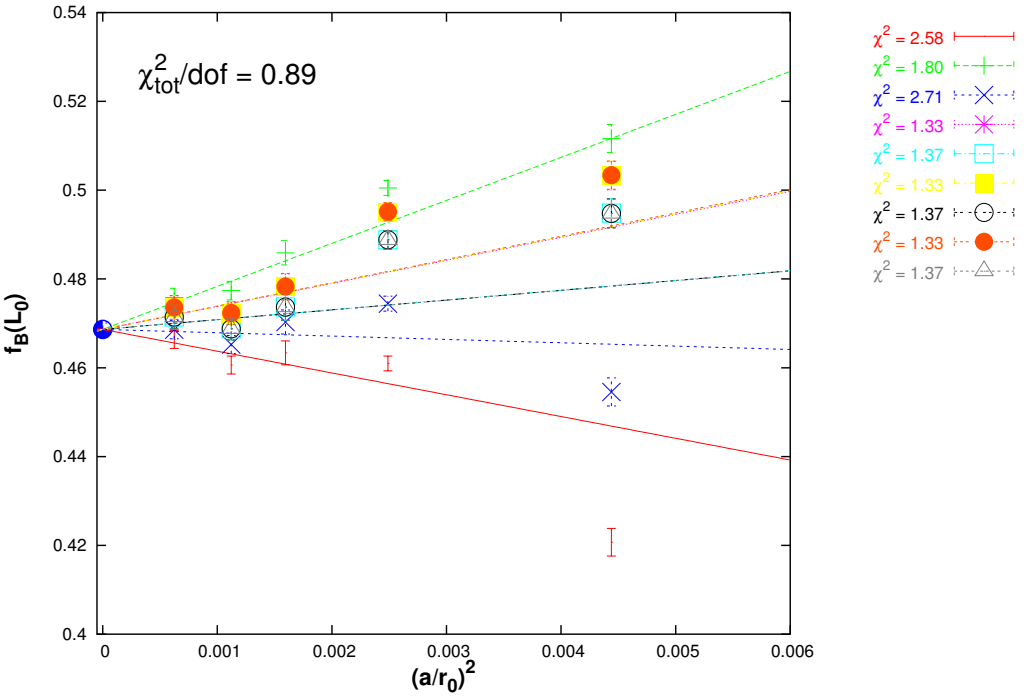

Figure 3.1: Continuum extrapolation on the small volume of $f_{B_s}(L_0)$. The different values of the decay constant correspond to different definitions of the RGI quark masses given in equations (2.32), (2.33) and (2.34). For each definition the two points at largest lattice spacing has been shown but not included in the fit. Units are in GeV.

$$\sigma_{h\ell}(L) = \lim_{a \mapsto 0} \Sigma_{h\ell}(L, a) \tag{3.5}$$

3.2.1 Small volume

Simulations of the decay constants on the smallest volume ($L_0 = 0.4$ fm) have been performed at five different lattice spacings using the geometries 24×12^3, 32×16^3, 40×20^3, 48×24^3 and 64×32^3 thus adding two more discretizations with respect to the calculation of the quark masses. For each discretization, a set of eight quark masses have been simulated. Two of the heavy masses have been chosen around the bottom quark $m_b^{RGI} = 6.73(16)$ GeV [2]. Other two have been chosen in the region of the charm quark $m_c^{RGI} = 1.681(36)$ [2]. An additional heavy quark has been simulated with mass 4.00 GeV. Three

light quark have been simulated with RGI masses of 0.14 GeV, 0.10 GeV and 0.06 GeV. Using the accurate determination of the RGI strange quark mass given in [42] one of the simulated light quarks has been chosen with the same mass of the physical s. The results of this finite volume calculation will be combined with the ones of the step scaling functions to provide results for the heavy–light decay constants with light quarks with masses around that of the strange. The final numbers will be in the continuum and on a large volume. All the parameters of the five different simulations are summarized in **Table** [**3.1**].

Different set of data have been obtained by using the different definitions of the RGI quark masses given in equations (2.32), (2.33) and (2.34). The continuum results have been extracted trough a combined fit of all the set of data, linear in $(a/r_0)^2$, as shown in **Figure** [**3.1**] in the case of the $\overline{b}s$ meson. For each set of data the three points nearest to the continuum have been included in the fit obtaining a global $\chi^2/dof = 0.89$ to be compared with the χ^2s of each individual definition listed in the figure. On this small volume, it is legitimate to use perturbative values for the improvement coefficient b_A since the values of the bare couplings used in the simulations are small ($g_0^2 \sim 0.85$). The systematics introduced in the calculation by the continuum extrapolations have been estimated repeating the fits linear in $(a/r_0)^2$ including, for each set of data, only the two points nearest to the continuum. The resulting systematic error has been found to be of the order of 1%. This error will be given to the results on the large volume added in quadrature with an error of about 2% coming from the uncertainties on the lattice spacing and on the renormalization factors. The latter have been evaluated by moving the points as a consequence of the change, within the errors, of the lattice spacings and of the renormalization constants and by repeating the whole analysis.

The finite volume results are:

$$f_{B_s}(L_0) = 475(2)MeV \qquad f_{D_s}(L_0) = 644(3)MeV \tag{3.6}$$

The errors quoted at this stage are statistical only, evaluated by a jackknife procedure. Due to the compression of the low energy scale, these results are higher than the large volume ones obtained after the step scaling functions multiplication chain (see eqs. (3.9) and (3.10)).

3.2.2 First volume step

The finite volume effects on the decay constants calculated on L_0, are measured by doubling the volume, $L_1 = 0.8$ fm, and by using the step scaling

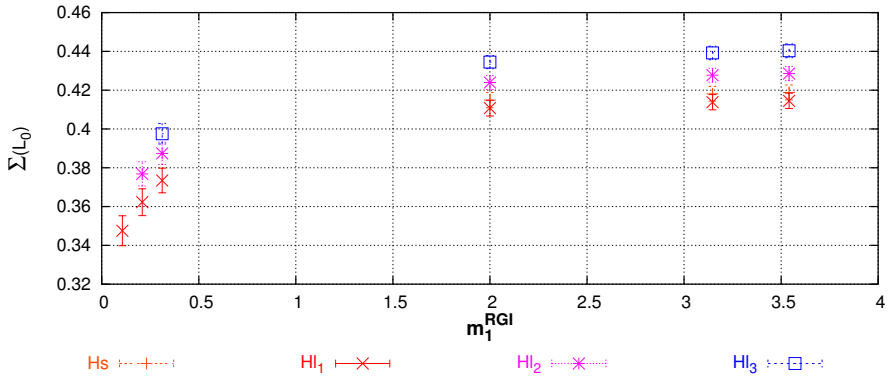

Figure 3.2: The figure shows the step scaling functions $\Sigma(L_0)$ as functions of m_1^{RGI}, for the simulation of the first evolution step corresponding to $\beta = 6.963$. The different sets of data correspond to the values of m_2^{RGI}. As can be seen the step scaling functions approach a plateau for high values of m_1^{RGI}. Similar plots can be obtained for the other values of the bare couplings.

function of eq (3.5).

The continuum extrapolations have been obtained by simulating the step scaling functions with three different discretizations of L_0, i.e 16×8^3, 24×12^3 and 32×16^3. The volume L_1 has been simulated starting from the discretizations of L_0, fixing the value of the bare coupling and doubling the number of lattice points in each direction.

The simulated quark masses have been halved with respect to the masses simulated on the small volume in order to have the same amount of discretization effects proportional to am. The set of parameters for the simulations of this evolution step is reported in **Table** [**3.2**]. The step scaling functions at $\beta = 6.963$ are plotted, at fixed m_2^{RGI}, as functions of m_1^{RGI} in **Figure** [**3.2**]. As can be seen, $\Sigma(L_0)$ is almost flat in a region of heavy quark masses starting around the charm mass. The hypothesis of low sensitivity upon the high–energy scale is thus verified. The value of the step scaling functions for the s quark are obtained trough linear interpolation. In **Figure** [**3.3**] are reported the results of the continuum extrapolation of the step scaling function, $\Sigma(L_0)$, of the pseudoscalar $\overline{h}s$ meson corresponding to the heaviest quark simulated in this step ($m_h^{RGI} = 3.55$ GeV). The residual heavy mass dependence of the continuum extrapolated step scaling functions is very mild, as shown in **Figure** [**3.4**] in the plot of σ_{B_s} as a function of the inverse quark mass. The continuum results are linearly extrapolated at the values of the heavy quark masses used in the small volume simulations.

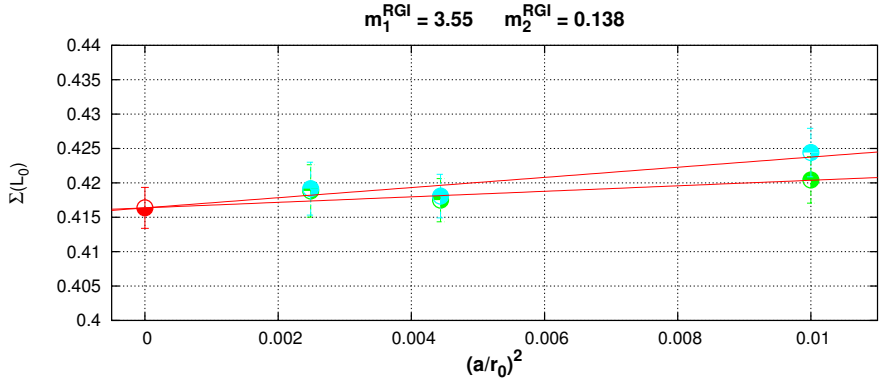

Figure 3.3: Continuum extrapolation on the first evolution step, $L_0 \mapsto L_1$, of the step scaling function, $\Sigma(L_0)$, of the pseudoscalar meson corresponding to the heavy quark of mass $m_1^{RGI} = 3.55$ GeV and to the s–quark. The two sets of data are obtained using the two definitions of RGI quark masses of equations (2.32) and (2.34). Units are in GeV. Similar plots can be obtained for the other combinations of quark masses used in the simulations.

The numbers obtained at this step are:

$$\sigma_{B_s}(L_0) = 0.417(3) \qquad \sigma_{D_s}(L_0) = 0.414(3) \tag{3.7}$$

The step scaling functions are free from the systematic errors coming from uncertainties on Z_A and b_A since the multiplicative improvement and renormalization factors cancel exactly in the ratio, being the numerator and the denominator evaluated at the same lattice spacing.

3.2.3 Second volume step

In order to have results on a physical volume, $L_2 = 1.6$ fm, as in the case of the meson masses, a second evolution step has been necessary. This is done computing the step scaling functions of eq. (3.5) at $L = L_1$, by the procedure outlined in the previous section. The parameters of the simulations are given in **Table** [**3.3**].

Also in this case, the values of the simulated quark masses have been halved with respect to the previous step, owing to the lower values of the simulation cutoffs. Even if the values of the quark masses have been lowered again, the linear extrapolations at the values of the heavy quark masses used on the small volume appears to be still valid and under control; see

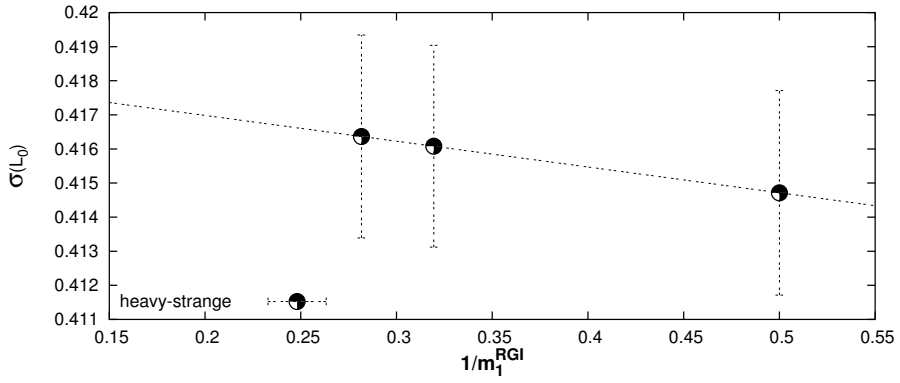

Figure 3.4: The figure shows the continuum extrapolated step scaling functions $\sigma(L_0)$ as functions of $1/m_1^{RGI}$. The heavy extrapolations are shown only for the $\overline{h}s$ set of data.

Figure [**3.5,3.7**]. This outcome have been predicted in section 1.2 by using dimensional analysis arguments. The value of the step scaling functions for the s quark have been obtained trough linear interpolation. **Figure** [**3.6**] shows the continuum extrapolation of the step scaling function, $\Sigma(L_1)$, of the $\overline{h}s$ meson corresponding to the heaviest quark simulated in this step ($m_h^{RGI} = 2.00$ GeV).

The numbers for this step are:

$$\sigma_{B_s}(L_1) = 0.97(3) \qquad \sigma_{D_s}(L_1) = 0.90(2) \tag{3.8}$$

The step scaling functions do not differ to much from one suggesting that an additional volume step it is not required.

3.3 Physical results

In this section the results of the small volume are combined with those of the step scaling functions to obtain, according to eq. (1.1), the physical numbers. In the end, the following physical results are obtained:

$$f_{B_s} = 192(6)(4) \text{ MeV} \qquad f_{D_s} = 240(5)(5) \text{ MeV} \tag{3.9}$$

The first error is statistical while the second one is an estimate of the systematics due to the uncertainties on the continuum extrapolations, on the scale and on the renormalization factors, as already discussed in sec. 3.2.1. The

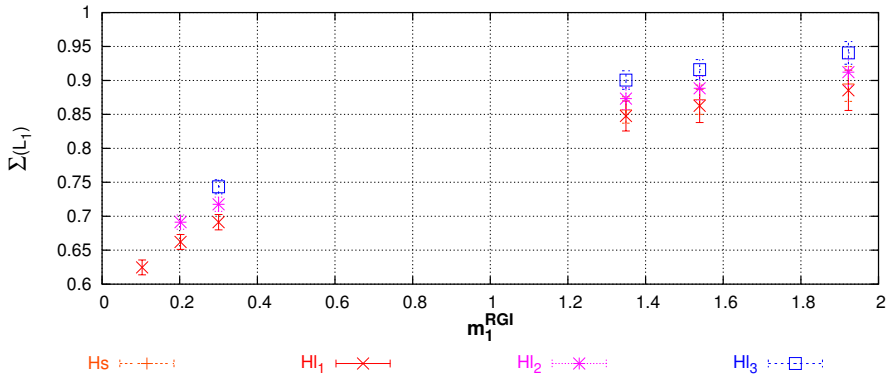

Figure 3.5: The figure shows the step scaling functions $\Sigma(L_1)$ as functions of m_1^{RGI}, for the simulation of the first evolution step corresponding to $\beta = 6.420$. The different sets of data correspond to the values of m_2^{RGI}. As can be seen the step scaling functions approach a plateau for high values of m_1^{RGI}. Similar plots can be obtained for the other values of the bare couplings.

value for f_{D_s} agrees with the average of dedicated calculations performed on large volumes [47, 48]. This result validates the choice of stopping the recursion at $L = 1.6$ fm that, of course, could have been explicitly checked to be safe by performing further evolution steps.

The chiral behavior of heavy–light pseudoscalar decay constants has been shown [49, 50, 51, 52] to contain logarithmic terms (χ–logs) that are diverging in the chiral limit, at variance with the unquenched case where these terms only affect the form of the extrapolation. In **Figure** [**3.8**] are shown the chiral extrapolations of the continuum heavy–light pseudoscalar decay constants. The data corresponding to the different values of the parameter Λ have been extrapolated using the parametrization suggested in [52]. As can be seen from the figure, the presence of the unphysical quenched χ–logs make the extrapolations unreliable down to the u–quark mass while the strange region seems to be dominated by a linear behavior. Nevertheless, in the literature values extrapolated linearly in the light quark mass have been quoted. For a *historical* comparison here below are given the corresponding results obtained in the present calculation:

$$f_B^{linear} = 171(8)(4)\ \text{MeV} \qquad f_D^{linear} = 221(7)(5)\ \text{MeV}$$

$$\frac{f_{B_s}}{f_B^{linear}} = 1.12(2)(1) \qquad \frac{f_{D_s}}{f_D^{linear}} = 1.09(1)(1) \tag{3.10}$$

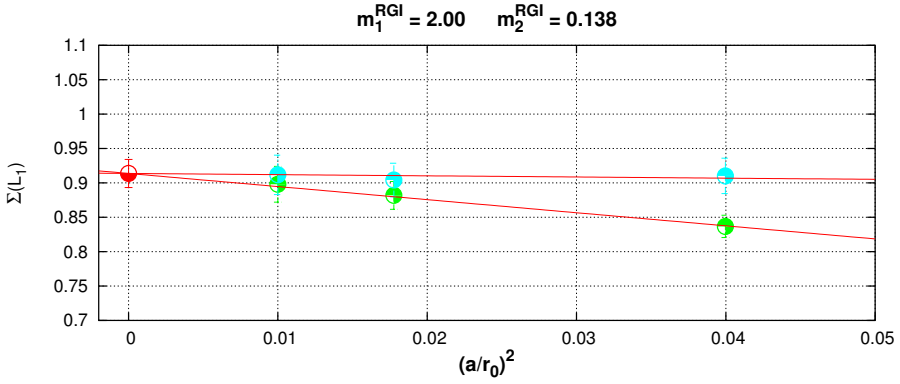

Figure 3.6: Continuum extrapolation on the first evolution step, $L_1 \mapsto L_2$, of the step scaling function, $\Sigma(L_1)$, of the pseudoscalar meson corresponding to the heavy quark of mass $m_1^{RGI} = 2.00$ GeV and to the s–quark. The two sets of data are obtained using the two definitions of RGI quark masses of equations (2.32) and (2.34). Units are in GeV. Similar plots can be obtained for the other combinations of quark masses used in the simulations.

that differ by a large factor from the unreliable values obtained from the fits shown in **Figure** [**3.8**] because of the diverging χ–logs.

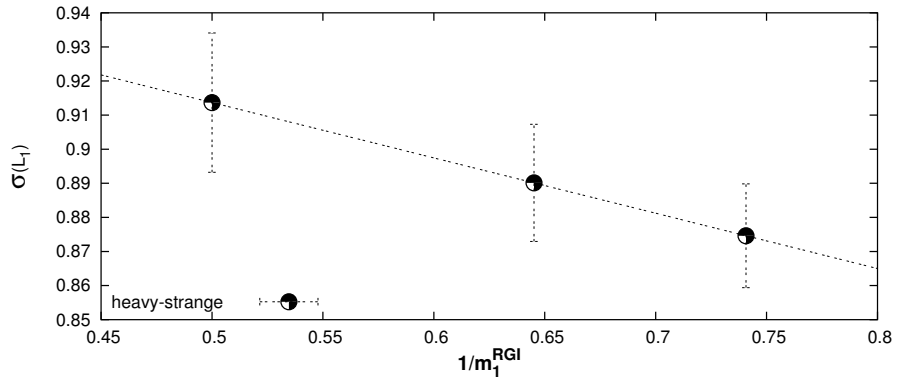

Figure 3.7: The figure shows the continuum extrapolated step scaling functions $\sigma(L_1)$ as functions of $1/m_1^{RGI}$. The heavy extrapolations are shown only for the $\overline{h}s$ set of data.

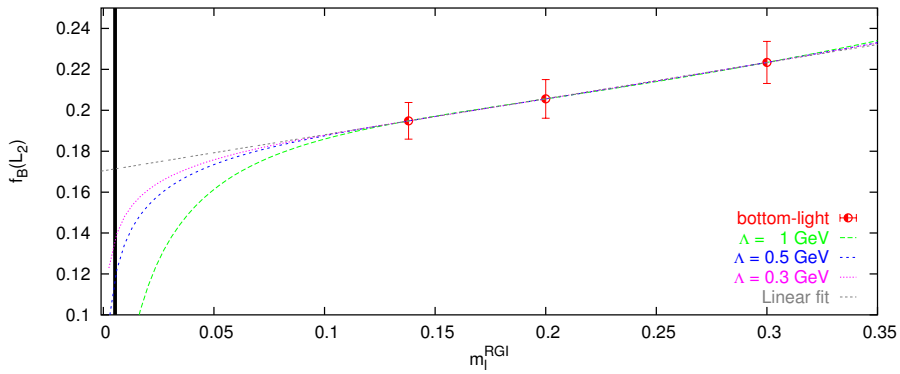

Figure 3.8: Chiral extrapolation of the continuum results for the pseudoscalar decay constants on the large volume. Units are in GeV.

β	L_0/a	k_c	k	m^{RGI} (GeV)
6.737	12	0.13520(1)	0.115528	7.51(9)
			0.116762	6.91(8)
			0.123555	4.019(43)
			0.130384	1.702(20)
			0.130089	1.604(18)
			0.134801	0.1347(31)
			0.134925	0.0929(29)
			0.135048	0.0513(29)
6.963	16	0.134827(6)	0.120081	7.14(8)
			0.120988	6.63(7)
			0.126050	4.024(44)
			0.131082	1.696(19)
			0.131314	1.591(18)
			0.134526	0.1381(30)
			0.134614	0.0978(28)
			0.134702	0.0574(28)
7.151	20	0.134492(5)	0.122666	7.03(11)
			0.123437	6.53(10)
			0.127605	3.97(6)
			0.131511	1.716(27)
			0.131686	1.617(25)
			0.134277	0.1257(36)
			0.134350	0.0829(33)
			0.134422	0.0407(32)
7.300	24	0.134235(3)	0.124176	7.11(8)
			0.124844	6.61(20)
			0.128440	4.018(44)
			0.131800	1.695(19)
			0.131950	1.592(18)
			0.134041	0.1374(27)
			0.134098	0.0971(24)
			0.134155	0.0567(24)
7.548	32	0.133838(2)	0.126352	7.10(8)
			0.126866	6.60(7)
			0.129585	4.016(44)
			0.132053	1.698(19)
			0.132162	1.595(18)
			0.133690	0.1422(27)
			0.133732	0.1021(25)
			0.133773	0.0618(23)

Table 3.1: Simulation parameters at $L_0 = 0.4$ fm. The RGI quark masses are obtained using eq. (2.32).

β	L_0/a	k_c	k	m^{RGI} (GeV)
6.420	8	0.135703(9)	0.120674	3.543(39)
			0.122220	3.114(34)
			0.126937	1.927(21)
			0.134304	0.3007(36)
			0.134770	0.2003(28)
			0.135221	0.1028(21)
6.737	12	0.135235(5)	0.1249	3.542(39)
			0.1260	3.136(34)
			0.1293	1.979(22)
			0.1343	0.3127(38)
			0.1346	0.2090(28)
			0.1349	0.1080(21)
6.963	16	0.134832(4)	0.127074	3.549(39)
			0.127913	3.153(35)
			0.130409	2.003(22)
			0.134145	0.3134(38)
			0.134369	0.2112(28)
			0.134593	0.1086(20)

Table 3.2: Simulation parameters for the first evolution step $L_0 \to L_1 = 0.8$ fm. The RGI quark masses are obtained using eq. (2.32).

β	L_1/a	k_c	k	m^{RGI} (GeV)
5.960	8	0.13490(4)	0.118128	2.012(22)
			0.121012	1.551(17)
			0.122513	1.337(15)
			0.131457	0.3154(36)
			0.132335	0.2322(28)
			0.133226	0.1466(44)
6.211	12	0.135831(8)	0.124090	1.984(22)
			0.126198	1.584(17)
			0.127280	1.389(15)
			0.133574	0.3493(39)
			0.134177	0.2550(29)
			0.134786	0.1510(19)
6.420	16	0.135734(5)	0.126996	1.933(21)
			0.128646	1.547(17)
			0.129487	1.355(14)
			0.134318	0.3016(34)
			0.134775	0.2038(24)
			0.135235	0.1055(15)

Table 3.3: Simulation parameters for the first evolution step $L_1 \to L_2 = 1.6$ fm. The RGI quark masses are obtained using eq. (2.32).

Part II

Boundary Conditions

Chapter 4

One–particle states

The study of quantum field theories on a finite volume is motivated by both theoretical and phenomenological reasons. In particular, a finite volume is required when the lattice regularization is adopted. The choice of the lattice regularization with respect to other useful continuum schemes is motivated by the fact that it is mathematically well defined from the beginning, it offers the unique opportunity to study non–perturbatively and from first principles a given quantum field theory and also because it has been shown to be the only known regularization to be able to account, in the case of vector–like theories, at the same time for gauge and the chiral invariance (see [53] for a complete introduction to chiral gauge theories on the lattice).

In their numerical applications lattice gauge theories are formulated in a finite 4–dimensional volume $T \times L^3$. The introduction of a low energy scale $(1/L)$ does regulate possible infrared divergences arising in the theory but it has also the consequence that the allowed physical momenta come out to be discretized in units of $2\pi/L$. The discretization of 3–momentum leads to a series of complications in the phenomenological applications of the lattice. A simple example in which such problems arise is represented by the two body decay of a given particle parametrized by the following matrix element

$$\mathcal{M}_{(A\to BC)} = {}_{out}\langle\ B(p_B)\ C(p_C)\ |\ A(p_A)\ \rangle_{in} \tag{4.1}$$

In this case the energies of the decay products are fixed by 4–momentum conservation but, because of the discretization of the 3–momenta, $\vec{p}_B$ and $\vec{p}_C$ cannot assume their physical values unless the masses of the three particles involved in the decay are chosen in such a way to fulfill the quantization rule.

In this chapter it is described a simple method devised in order to overcome some of these difficulties. The key points are that the momentum

quantization condition depends upon the choice of the boundary conditions and that different particles species (different fields) can have different boundary conditions. By using these simple observations it is possible to handle in lattice simulations physical momenta smaller than the lowest allowed excitation $(2\pi/L)$ in the case of standard periodic boundary conditions for all the fields.

4.1 Periodic fields

In this section it is briefly reviewed the derivation of the momentum quantization rule in the case of a field satisfying periodic boundary conditions (PBC) on a finite volume $T \times L^3$. In the following no hypotheses are made on the boundary conditions satisfied by the field $\psi(x)$ in the time direction while, in the spatial directions, $\psi(x)$ is required to satisfy

$$\psi(x + \vec{e}_i \; L) = \psi(x) \; , \qquad i = 1, 2, 3 \tag{4.2}$$

This condition can be re–expressed by Fourier transforming both members of the previous equation

$$\int d^4p \; e^{-ip(x+\vec{e}_i \; L)} \; \tilde{\psi}(p) = \int d^4p \; e^{-ipx} \; \tilde{\psi}(p) \; , \qquad i = 1, 2, 3 \tag{4.3}$$

It follows directly from the previous relation that, in the case of periodic boundary conditions, one has

$$e^{ip_i L} = 1 \quad \Longrightarrow \quad p_i = \frac{2\pi \; n_i}{L} \; , \quad i = 1, 2, 3 \tag{4.4}$$

where the n_i's are integer numbers. As already mentioned, the first allowed momentum on a volume of the order of 2 fm is given by

$$p = \frac{2\pi}{L} \simeq 600 \text{ MeV} \qquad\qquad L \simeq 2 \text{ fm} \tag{4.5}$$

and it is usually not possible to explore the interesting kinematic region of a given physical process by varying the particle momenta by quanta of 0.6 GeV.

4.2 θ–periodic fields

The authors of refs. [54, 55, 56, 57, 58, 59, 60, 61] have considered a generalized set of boundary conditions, in the following referred to as θ–boundary conditions (θ–BC), depending upon the choice of a topological 3–vector $\vec{\theta}$

$$\psi(x + \vec{e}_i \; L) = e^{-i\theta_i} \; \psi(x) \; , \qquad i = 1, 2, 3 \tag{4.6}$$

The modification of the boundary conditions shifts the zero of the momenta. Indeed, by re–expressing equation (4.6) in Fourier space, as already done in the case of PBC in equation (4.3), one has

$$\int d^4p\ e^{-ip(x+\vec{e}_i\ L)}\ \tilde{\psi}(p) = \int d^4p\ e^{-i(px+\theta_i)}\ \tilde{\psi}(p)\ , \qquad i=1,2,3 \tag{4.7}$$

form which

$$e^{i(p_i-\frac{\theta_i}{L})L} = 1 \quad \Longrightarrow \quad p_i = \frac{\theta_i}{L} + \frac{2\pi\ n_i}{L}\ , \quad i=1,2,3 \tag{4.8}$$

It comes out that the spatial momenta are still quantized as for PBC but shifted by the amount (θ_i/L). The observation that this continuous shift in the allowed momenta is physical and can thus be profitably used in phenomenological applications is the key point of this chapter (see also ref. [4]).

4.3 Bloch's theorem and θ–BC

The physical meaning of θ–boundary conditions can be clarified by analogy with the wavefunction of an electron in a crystal. Indeed, a quark on the lattice experiences a periodic potential as well as the electron does in a solid and they both satisfy the Dirac equation. The analogy is completed by identifying the lattice extension L with the extension of the unit cell (that unfortunately is often called a as the lattice spacing) and not with the linear extension of the crystal. The well known Bloch's theorem holds

theorem 1 *The wavefunctions of the "crystal Hamiltonian" can be written as the product of a plane wave of wave-vector $\vec{k}$ from within the first Brillouin zone, times an appropriate periodic function:*

$$\psi_{\vec{k}}(\vec{r}) = e^{i\vec{k}\cdot\vec{r}}\ u_{\vec{k}}(\vec{r}) \tag{4.9}$$

where

$$u_{\vec{k}}(\vec{r}+\vec{n}L) = u_{\vec{k}}(\vec{r}) \qquad \textit{and} \qquad 0 \le k_i < \frac{2\pi}{L} \tag{4.10}$$

It should be noted that the wavefunctions $\psi_{\vec{k}}(\vec{r})$ do not satisfy periodic boundary conditions but the more general b.c.'s

$$\psi_{\vec{k}}(\vec{r}+\vec{n}L) = e^{i\vec{k}\cdot\vec{n}L}\ \psi_{\vec{k}}(\vec{r}) \tag{4.11}$$

These boundary conditions are identical to those introduced in the previous section and the complete matching is obtained by recognizing

$$\vec{k} = \frac{\vec{\theta}}{L} \tag{4.12}$$

4.4 Numerical implementation

The generalized θ–dependent boundary conditions of equation (4.6) can be implemented in lattice simulations in a simple way. It useful to consider a unitary Abelian transformation on the fields satisfying θ–BC

$$\psi(x) \quad \longrightarrow \quad \mathcal{U}\ (\theta, x)\psi(x) = e^{-\frac{i\theta x}{L}}\ \psi(x) \tag{4.13}$$

As a consequence of this transformation the resulting field satisfies periodic boundary conditions but obeys a modified Dirac equation

$$\begin{aligned} S[\bar{\psi}, \psi] \quad &\longrightarrow \quad \sum_{x,y} \bar{\psi}(x)\ \mathcal{U}(\theta, x) D(x, y) \mathcal{U}^{-1}(\theta, y)\ \psi(y) \\ &= \quad \sum_{x,y} \bar{\psi}(x)\ D_\theta(x, y)\ \psi(y) \end{aligned} \tag{4.14}$$

where the θ–dependent lattice Dirac operator $D_\theta(x, y)$ is obtained by starting from the preferred discretization of the Dirac operator and by modifying the definition of the covariant lattice derivatives, i.e. by passing from the standard forward and backward derivatives:

$$\begin{aligned} \nabla_\mu \psi(x) &= \frac{1}{a} \left[U_\mu(x) \psi(x + a\ \hat{\mu}) - \psi(x) \right] \\ \nabla^\star_\mu \psi(x) &= \frac{1}{a} \left[\psi(x) - U^{-1}_\mu(x - a\ \hat{\mu}) \psi(x - a\ \hat{\mu}) \right] \end{aligned} \tag{4.15}$$

to the θ–dependent ones

$$\begin{aligned} \nabla_\mu(\theta) \psi(x) &= \frac{1}{a} \left[\lambda_\mu\ U_\mu(x) \psi(x + a\ \hat{\mu}) - \psi(x) \right] \\ \nabla^\star_\mu(\theta) \psi(x) &= \frac{1}{a} \left[\psi(x) - \lambda^{-1}_\mu\ U^{-1}_\mu(x - a\ \hat{\mu}) \psi(x - a\ \hat{\mu}) \right] \end{aligned} \tag{4.16}$$

where

$$\lambda_\mu = e^{\frac{ia\theta_\mu}{L}} \qquad\qquad \theta_0 = 0 \tag{4.17}$$

4.5 A simple numerical test

The physical significance of $\vec{\theta}/L$ as a true physical momentum can be checked by performing a simple numerical test. It has been calculated the energy of a meson made up of two different quarks with different θ–BC for the two flavors. The work has been done by using the $O(a)$–improved Wilson–Dirac lattice formulation of the QCD within the Schrödinger Functional formalism (see sections 2.1 and 2.2) but, as already mentioned, the use of θ–BC in the spatial directions is completely decoupled from the choice of time boundary conditions and can be profitably used also outside the Schrödinger Functional formalism, for example when using standard periodic time boundary conditions. The following correlators have been considered

$$f_P^{ij}(\theta; x_0) = -\frac{a^6}{2} \sum_{\vec{y},\vec{z},\vec{x}} \langle\ \bar{\zeta}_i(\vec{y})\gamma_5\zeta_j(\vec{z})\ \bar{\psi}_j(x)\gamma_5\psi_i(x)\ \rangle \tag{4.18}$$

where i and j are flavor induces, all the fields satisfy periodic boundary conditions and the two flavors obey different θ–modified Dirac equations, as explained in equations (4.14), (4.15) and (4.16). In practice it is adequate to choose the flavor i with $\theta = 0$, i.e. with ordinary PBC, and the flavor j with $\theta \neq 0$. After the Wick contractions the pseudoscalar correlator of equation (4.18) reads

$$f_P^{ij}(\theta; x_0) = \frac{a^6}{2} \sum_{\vec{y},\vec{z},\vec{x}} \mathrm{Tr}\,\langle\ \gamma_5\ S_j(\theta; \vec{z}, x)\ \gamma_5\ S_i(0; x, \vec{y})\ \rangle \tag{4.19}$$

where $S(\theta; x, y)$ and $S(0; x, y)$ are the inverse of the θ–modified and of the standard Wilson–Dirac operators respectively. Note that the projection on the momentum $\vec{\theta}/L$ of one of the quark legs in equation (4.19) it is not realized by summing on the lattice points with an exponential factor but it is encoded in the θ–dependence of the modified Wilson–Dirac operator and, consequently, of its inverse $S(\theta; x, y)$.

This correlation is expected to decay exponentially at large times as

$$f_P^{ij}(\theta; x_0) \qquad \overset{x_0 \gg 1}{\longrightarrow} \qquad f_{ij}\ e^{-a x_0 E_{ij}(\theta, a)} \tag{4.20}$$

where, a part from corrections proportional to the square of the lattice spacing, E_{ij} is the physical energy of the meson state

$$E_{ij}(\theta, a) = \sqrt{M_{ij}^2 + \left(\frac{\vec{\theta}}{L}\right)^2} + O(a^2) \tag{4.21}$$

β	$\mathbf{L/a}$	$\mathbf{k}$	$\mathbf{r_0\ m^{RGI}}$
5.960	16	0.132054	0.645(7)
		0.132609	0.520(6)
		0.133315	0.362(5)
		0.133725	0.269(4)
6.211	24	0.134208	0.655(9)
		0.134540	0.521(7)
		0.134954	0.354(6)
		0.135209	0.251(5)
6.420	32	0.134517	0.676(15)
		0.134764	0.540(12)
		0.135082	0.365(10)
		0.135269	0.262(9)
$[\theta_\mathbf{x}, \theta_\mathbf{y}, \theta_\mathbf{z}]$ =	[0.0, 0.0, 0.0]	[1.0, 1.0, 1.0]	[2.0, 2.0, 2.0]	[3.0, 3.0, 3.0]

Table 4.1: Parameters of the simulations. The values of the bare couplings has been chosen in order to fix the extension of the physical volume $L = 3.2\ r_0$. For each value of the k parameter all the values of $\vec{\theta}$ have been simulated.

here M_{ij} is the mass of the pseudoscalar meson made of a i and a j quark anti–quark pair. After the continuum extrapolations the expected relativistic dispersion relations have to be recovered

$$E_{ij}^2 = M_{ij}^2 + \left(\frac{\vec{\theta}}{L}\right)^2 \tag{4.22}$$

see **Figure** [**4.2**].

4.5.1 Simulations

All the results of this section have been obtained in the quenched approximation of the QCD. A physical volume of topology $T \times L^3$ with $T = 2L$ and linear extension $L = 3.2\ r_0$ has been simulated (see section 2.6). In order to extrapolate numerical results to the continuum limit the same physical volume has been simulated by using three different discretizations with 32×16^3, 48×24^3 and 64×32^3 points respectively. The bare couplings corresponding to the different discretizations have been fixed by using the r_0 scale with the numerical results given in [40]. All the parameters of the simulations are given in **Table** [**4.1**]. The values of the RGI quark masses reported in **Table** [**4.1**] have been calculated according to equation (2.32). For each value of the simulated quark masses reported in **Table** [**4.1**] the Wilson–Dirac operator has been inverted for three non–zero values of $\vec{\theta}$. Setting the lattice

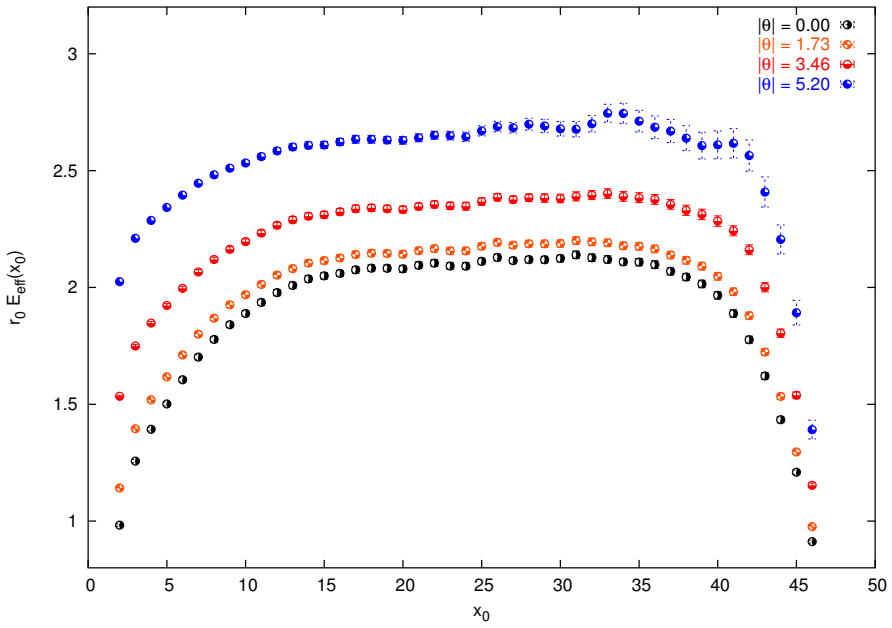

Figure 4.1: Effective energies $E^{ij}_{eff}(\theta, a; x_0)$, as defined in eq. (4.24) at fixed cut–off. The results correspond to the simulation done at $\beta = 6.211$ with $r_0\ m_1^{RGI} = 0.655$ and $r_0\ m_2^{RGI} = 0.354$. Similar figures could have been shown for other combinations of the simulated quark masses and for the other values of the bare coupling.

scale by using the physical value $r_0 = 0.5$ fm, the expected values of the physical momenta associated with the choices of $\vec{\theta}$ given in **Table** [**4.1**] are simply calculated according to the following relation

$$|\vec{p}| \ = \ \frac{|\vec{\theta}|}{L} \ \simeq \ 0.125\ |\vec{\theta}|\ \text{GeV} \quad = \quad \left\{ \begin{array}{l} 0.000 \\ 0.217 \\ 0.433 \\ 0.650 \end{array} \right. \ \text{GeV} \qquad L \ \simeq \ 1.6\ \text{fm} \quad (4.23)$$

These values have to be compared with the value of the lowest physical momentum allowed on this finite volume in the case of periodic boundary conditions, i.e. $|\vec{p}| \simeq 0.785$ GeV.

At fixed cut–off, for each combination of flavor indexes and for each value of $\vec{\theta}$ reported in **Table** [**4.1**] was extracted the effective energy from the correlations of eq. (4.18), $f^{ij}_P(\theta; x_0)$, as follows

$$a\ E^{ij}_{eff}(\theta, a; x_0) \ = \ \frac{1}{2}\ \log\left(\frac{f^{ij}_P(\theta; x_0 - 1)}{f^{ij}_P(\theta; x_0 + 1)}\right) \qquad (4.24)$$

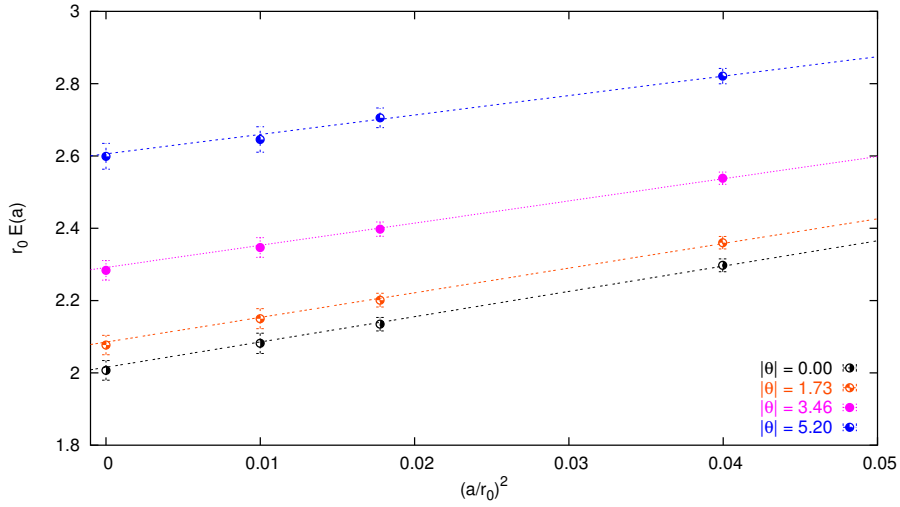

Figure 4.2: Continuum extrapolations of the plateau averaged effective energies $E^{ij}(\theta, a)$. The results correspond to the quark masses $r_0\ m_1^{RGI} = 0.650$ and $r_0 m_2^{RGI} = 0.350$. Similar figures could have been shown for other combinations of the simulated quark masses.

In **Figure** [**4.1**] this quantity is shown for the simulation performed at $\beta = 6.211$ corresponding to $r_0\ m_1^{RGI} = 0.655$ and $r_0\ m_2^{RGI} = 0.354$, for each simulated value of $\vec{\theta}$. As can be seen, the energies with higher values of $|\vec{\theta}|$ are always greater than the corresponding ones with lower values of the physical momentum

$$|\vec{\theta}_1| > |\vec{\theta}_2| \quad \Rightarrow \quad E^{ij}_{eff}(\theta_1, a; x_0) > E^{ij}_{eff}(\theta_2, a; x_0) \tag{4.25}$$

a feature that is confirmed in the continuum limit, as discussed below.

In the continuum extrapolations the physical values of the quark masses have been fixed by slightly interpolating the simulated sets of numerical results. The effective energies have been averaged over a ground state plateau of physical length depending upon the quark flavors. The result of the average is referred to as $E^{ij}(\theta, a)$ and in **Figure** [**4.2**] a typical continuum extrapolation of this quantity is shown. Similar figures could have been shown for the other values of simulated quark masses.

The continuum results verify very well the dispersion relations of equation (4.22) as can be clearly seen from **Figure** [**4.3**] in which the square of $E^{ij}(\theta)$ for various combinations of the flavor indexes is plotted versus the square of the physical momenta $|\vec{\theta}|/L$. The plotted lines have not been fitted

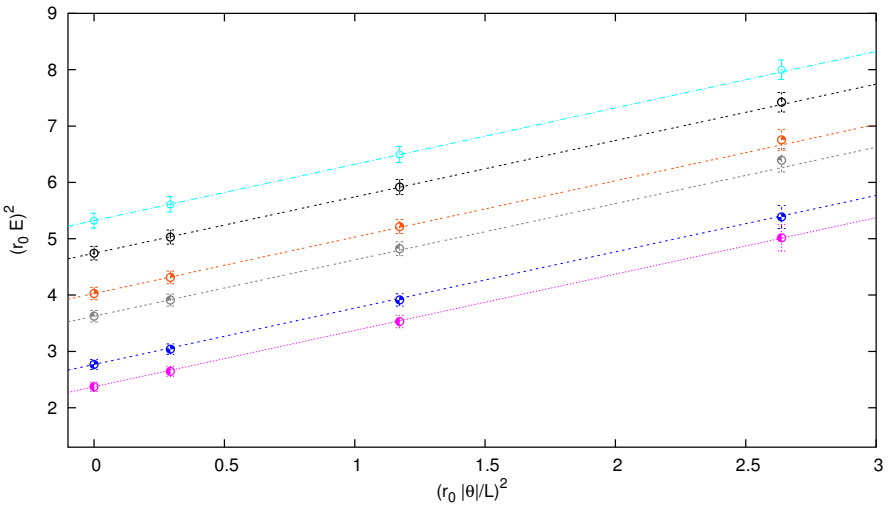

Figure 4.3: Continuum dispersion relations. The data correspond to different combinations of the simulated quark masses and reproduce very well the expected theoretical behavior, i.e. straight lines having as intercepts the meson masses and as angular coefficients one (see eq. 4.22).

but have been obtained by using as intercepts the simulated meson masses and by fixing their slope to one.

4.6 θ–BC vs. unquenched simulations

The usefulness of θ–boundary conditions in the case of unquenched simulations is limited by severe algorithmic limitations. The discussion of this section is restricted to the case of numerical simulations of a $N_f = 2$ theory but can be generalized to the case in which a larger number of dynamical fermions is included in the simulation.

Current unquenched simulation algorithms [62, 63, 64, 65, 66, 67, 68] include the effect of dynamical fermions by generating gauge configurations with the distribution

$$w[U] = \det D_1[U] \ \det D_2[U] \ e^{-S_G[U]} \tag{4.26}$$

where $S_G[U]$ is the gauge action while $D_1[U]$ and $D_2[U]$ are the discretized Dirac operators acting on $\psi_1(x)$ and $\psi_2(x)$ respectively. The determinants are evaluated by introducing bosonic fields, called "pseudo fermions", with

the action

$$S_{PF}[\overline{\phi}_1, \phi_1, \overline{\phi}_2, \phi_2, U] = \int d^4x \ \overline{\phi}_1(x) D_1^{-1} \phi_1(x) + \int d^4x \ \overline{\phi}_2(x) D_2^{-1} \phi_2(x) \tag{4.27}$$

The pseudo fermion action has to be non negative and this requirement puts stringent limits on the choice of the discretized version of the Dirac operator. When the Wilson–Dirac formulation is used the single $D_i[U]$ is not positive definite and the theory can be only simulated by considering two mass degenerate fermions with exactly the same operator

$$w[U] = (\det D[U])^2 \ \ e^{-S_G[U]} \tag{4.28}$$

and

$$S_{PF}[\overline{\phi}, \phi, U] = \int d^4x \ \overline{\phi}(x) D^{-2} \phi(x) \tag{4.29}$$

Hence, by using this formulation the two flavors must satisfy exactly the same Dirac equation and, consequently, it is not possible to chose different θ–angles for the different fermion species.

The problem can be overcome by considering a discrete formulation of the theory in which the single Dirac operator is non negative by its own. This is the case of the so called "Ginsparg–Wilson" (GW) formulations (for a recent review on GW fermions and a complete list of references see [69]) that have the great advantage to preserve exact chiral symmetry at finite lattice spacing. On the other hand, current algorithms to simulate GW fermions are extremely demanding in terms of computing power and are seldom used in phenomenological applications where θ–BC would be very useful.

Chapter 5

Scattering states

In the previous chapter the role played by the choice of the boundary conditions it has been extensively discussed in the case of one particle states on a finite volume. This chapter is dedicated to the study of the spectrum of two scattering particles on a finite volume in the case of θ–boundary conditions. The main result is the derivation of a quantization condition relating the energy of a scattering state on a finite volume with the infinite volume scattering phases. This condition is derived by matching the quantum field system with a simple quantum mechanical analog and can, in principle, be used to calculate the scattering phases when the energy of the state is known or vice versa.

A generalization of the so called Lellouch–Lüscher (LL) formula [70] it is also derived, connecting the finite volume amplitude for a two body non leptonic decay with the corresponding result in the infinite volume. This formula is a step toward the solution of the long standing problem of the explanation of the $\Delta I = 1/2$ puzzle in the decay of a kaon into two pions.

From the numerical point of view, the usefulness of the quantization condition and of the generalized LL formula, as given in this chapter, is strongly limited by two problems. The first one has been already discussed in the previous chapter and is related to the fact that different boundary conditions for the up and down quarks in unquenched simulations of lattice QCD cannot be chosen for Wilson fermions. The second problem has been pointed out in ref. [17] and concerns the breaking of the isospin symmetry by the choice of different θ–angles for the two light running quarks (see section 5.11). A possible solution to the isospin problem can be found by using a generalization of the KKR method discussed in this chapter by including in the calculation different two–particle states with different boundary conditions

(see section 5.2).

5.1 Two–particle states in a finite volume

The spectrum of a two–particle state on a finite volume in quantum field theory has been already studied in great detail in refs. [71, 72, 73, 74] in the case in which the two particles satisfy periodic boundary conditions. An energy quantization condition has been found by establishing in ref. [71, 75] a connection between quantum field theory and non–relativistic quantum mechanics. Indeed, by assuming that the two particles are spinless bosons of equal mass m whose dynamics can be described by a scalar field theory of the ϕ^4–type with unbroken reflection symmetry $\phi \mapsto -\phi$ and one–particle states odd under this symmetry, an effective Schrödinger equation can be written for the two–particle state. In the center-of-mass reference frame this equation reads

$$-\frac{1}{2\mu}\triangle\psi(\vec{r}) + \frac{1}{2}\int d\vec{r}'\ U_E(\vec{r},\vec{r}')\ \psi(\vec{r}') = E\psi(\vec{r}) \tag{5.1}$$

where the parameter E does not represent the true energy of the system, that here is called $\mathcal{E}$, but it is connected to the last through

$$\mathcal{E} = 2\sqrt{m^2 + mE} \tag{5.2}$$

In eq. (5.1) the parameter μ represent the reduced mass of the two–particle system while $U_E(\vec{r},\vec{r}')$ is the Fourier transform of the modified Bethe–Salpeter kernel $\hat{U}_E(\vec{k},\vec{k}')$ introduced in [71]. The "pseudo–potential" $U_E(\vec{r},\vec{r}')$ depends analytically on E in the range $-m < E < 3m$, is a smooth function of the coordinates $\vec{r}$ and $\vec{r}'$ decaying exponentially in each direction and is rotationally invariant so that one can pass to the radial effective Schrödinger equation.

Thanks to these observations, in the following the calculation of the spectrum of a two–particle state in a finite volume will be carried out by using a purely non–relativistic Hamiltonian that, separating the center of mass motion from the internal motion, comes out to depend upon the relative coordinate $\vec{r} = \vec{x} - \vec{y}$ only

$$\hat{H} = -\frac{1}{2\mu}\triangle + V(r), \qquad r = \|\vec{r}\| \tag{5.3}$$

where $\triangle$ is the Laplacian operator with respect to $\vec{r}$. The potential is assumed to be spherically symmetric, a smooth function of its argument and of finite range, i.e.

$$V(r) = 0 \qquad \text{for} \qquad r > R \tag{5.4}$$

The problem will be solved on a finite cubical box of linear extension L greater than the potential radius ($L > R$) in each direction. It will be assumed that the potential is periodic of period L

$$V(\|\vec{r} + \vec{n}L\|) = V(r) \qquad \text{for} \qquad \vec{n} \in \mathbf{Z}^3 \tag{5.5}$$

One can imagine to start from a given finite–range potential $\mathcal{V}(r)$ that describes the interactions of the two particles and to build a periodic potential as follows

$$V(\vec{r}) = \sum_{\vec{n}\in\mathbf{Z}^3} \mathcal{V}(\|\vec{r} + \vec{n}L\|) \tag{5.6}$$

By construction $V(\vec{r})$ satisfies the periodicity condition stated in eq. (5.5).

There are two differences between the potential $V(\vec{r})$ that has been introduced so far and the pseudo–potential $U_E(\vec{r}, \vec{r}')$. The first one concerns the energy dependence of U_E but this does not represent a problem because all the results will be obtained at fixed E. The second difference between the quantum field system and the non–relativistic one is that $U_E(\vec{r}, \vec{r}')$ does not vanish if either $\vec{r}$ or $\vec{r}'$ is greater than R, but it has exponentially small corrections. Furthermore in the quantum field system there are additional exponentially small finite volume corrections that arise from polarization effects. For these reasons the results derived in the non–relativistic theory retain their validity also in the relativistic theory up to exponentially small corrections.

The matching with a quantum mechanical system could have been avoided by following an approach similar to that developed in ref. [76]. In the following sections this strategy has not been pursued because, as will be clear later on, the quantum mechanical analogy allows one to benefit without additional effort of a series of theoretical results obtained in the framework of solid state physics and useful also in the present case.

5.2 Quantization condition

In this section a powerful relation, connecting the energy eigenvalues of a two–particle state on a finite volume with the infinite volume scattering phases of the two particles, it is derived. Thanks to the observations of the previous section the calculation is done in NRQM since the results retain their validity also in QFT up to exponentially vanishing finite volume corrections.

In order to obtain the energy quantization condition one has to solve the Schrödinger equation for a particle in a periodic potential, i.e. the same

equation satisfied by electrons, holes and excitons in a periodic crystal. Useful results well known to the solid state physics community since a long time can thus be exported to the present problem, provided the "cell size" of the crystal is interpreted as the physical extension of the finite volume, i.e. L.

It is useful to solve the problem by using θ–boundary conditions introduced in the previous chapter

$$\psi_{\vec{k}}(\vec{r}+\vec{n}L) = e^{i\vec{k}\cdot\vec{n}L}\ \psi_{\vec{k}}(\vec{r}) \tag{5.7}$$

or

$$\psi_{\vec{\theta}}(\vec{r}+\vec{n}L) = e^{i\vec{\theta}\cdot\vec{n}}\ \psi_{\vec{\theta}}(\vec{r}) \qquad\qquad \vec{k} = \frac{\vec{\theta}}{L} \tag{5.8}$$

As discussed in section 4.3 this choice of the boundary conditions finds its physical interpretation in terms of the well known Bloch's theorem 1.

5.2.1 Korringa–Kohn–Rostoker theory

Another fundamental result obtained within the context of solid state physics is the computational framework developed independently by Korringa [77], Kohn and Rostoker [78] and known as the KKR method or the Green's function method. This method can be straightforwardly used in the present calculation in order to derive the two–particle state energy quantization condition in a simple way.

The KKR method can be applied under the hypotheses of a so called "muffin thin potential", i.e. a periodic, spherical symmetric potential that vanishes beyond a given distance R within each cell of the crystal. All these hypotheses are satisfied by the potential defined in eq. (5.6). The KKR procedure starts by considering the time–independent form of the Schrödinger equation

$$\left(\triangle + q^2\right)\psi_{\vec{k}}(\vec{r}) = V'(\vec{r})\psi_{\vec{k}}(\vec{r}) \tag{5.9}$$

where it has been defined

$$q^2 = 2\mu E \tag{5.10}$$

and $2\mu V(\vec{r})$ has been substituted with $V'(\vec{r})$. In order to have a formal solution of this non–homogeneous partial differential equation it is customary to introduce the free–particle Green's function as the solution of

$$\left(\triangle_{\vec{r}} + q^2\right) g(\vec{r}-\vec{r}_0; q) = \delta(\vec{r}-\vec{r}_0) \tag{5.11}$$

The solution of eq. (5.9) can be formally written in terms of the Green's function as

$$\psi_{\vec{k}}(\vec{r}) = \phi_{\vec{k}}(\vec{r}) + \int_{-\infty}^{+\infty} d\vec{r}_0 \; g(\vec{r} - \vec{r}_0; q) V'(\vec{r}_0) \psi_{\vec{k}}(\vec{r}_0) \tag{5.12}$$

where $\phi_{\vec{k}}(\vec{r})$ is a solution of the homogeneous equation associated with eq. (5.9) with the additional requirement to satisfy the Bloch's condition of eq. (5.7). In the previous equation the integration variable $\vec{r}_0$ spans the whole three dimensional space and not only a period. In the rest of this section it will be assumed $\phi_{\vec{k}}(\vec{r}) = 0$ while the case in which the homogeneous solution is present will be discussed later on. Eq. (5.12) can be rewritten as

$$\psi_{\vec{k}}(\vec{r}) = \int_{-\infty}^{+\infty} d\vec{r}_0 \; g(\vec{r} - \vec{r}_0; q) V'(\vec{r}_0) \psi_{\vec{k}}(\vec{r}_0) \tag{5.13}$$

It should be observed that no particular conditions are requested to the Green's function in order $\psi_{\vec{k}}(\vec{r})$ to satisfy the Bloch's condition; indeed since $\psi_{\vec{k}}(\vec{r})$ is present in both the members of the previous equation and since the potential is periodic, the condition of eq. (5.7) is self–consistently satisfied. For this reason, $g(\vec{r} - \vec{r}_0; q)$ is not required to satisfy any particular periodicity condition and is given by

$$g(\vec{r} - \vec{r}_0; q) = -\frac{1}{4\pi} \frac{e^{iq\|\vec{r} - \vec{r}_0\|}}{\|\vec{r} - \vec{r}_0\|} \tag{5.14}$$

The domain of integration in eq. (5.13) can be reduced from the entire world to a single periodicity cell by introducing the "greenian" of the equation defined as

$$g_{\vec{k}}(\vec{r} - \vec{r}_0; q) = \sum_{\vec{n} \in \mathbf{Z}^3} e^{i\vec{k} \cdot \vec{n} L} g(\vec{r} - \vec{r}_0 - \vec{n} L; q) \tag{5.15}$$

Using the greenian definition together with the Bloch's condition and the periodicity of the potential, the formal solution of the Schrödinger equation can be rewritten as an integral spanning only a period

$$\psi_{\vec{k}}(\vec{r}) = \int_{\text{period}} d\vec{r}_0 \; g_{\vec{k}}(\vec{r} - \vec{r}_0; q) V'(\vec{r}_0) \psi_{\vec{k}}(\vec{r}_0) \tag{5.16}$$

but, since the potential is identically zero for distances greater than R, the integration domain can be further reduced to a sphere of radius R

$$\psi_{\vec{k}}(\vec{r}) = \int_{S_R} d\vec{r}_0 \; g_{\vec{k}}(\vec{r} - \vec{r}_0; q) V'(\vec{r}_0) \psi_{\vec{k}}(\vec{r}_0) \tag{5.17}$$

Thank to the Schrödinger equation (5.9), the previous relation can be rewritten in a form suitable for the application of the Green's theorem

$$\psi_{\vec{k}}(\vec{r}) = \int_{S_R} d\vec{r}_0 \; g_{\vec{k}}(\vec{r} - \vec{r}_0; q)(\triangle_{\vec{r}_0} + q^2)\psi_{\vec{k}}(\vec{r}_0) \tag{5.18}$$

Using the simple identity

$$g\triangle\psi = \psi\triangle g + \vec{\nabla} \cdot (g\vec{\nabla}\psi - \psi\vec{\nabla}g) \tag{5.19}$$

and the Green's theorem, a vanishing surface integral is finally obtained

$$\int_{\partial S_R} dS_0 \; \left[g_{\vec{k}}(\vec{r} - \vec{r}_0; q)\frac{\partial\psi_{\vec{k}}(\vec{r}_0)}{\partial r_0} - \psi_{\vec{k}}(\vec{r}_0)\frac{\partial g_{\vec{k}}(\vec{r} - \vec{r}_0; q)}{\partial r_0} \right]_{r_0=R} = 0 \tag{5.20}$$

The previous equation is the quantization condition that the wavefunction in the center–of–mass reference frame of a two particle state with θ–BC has to satisfy in a finite volume L^3. In the following, by using the expansion in spherical harmonics of both the greenian and the wavefunction, this condition will be shown to be equivalent to a system of equations expressing the two–particle scattering phases as functions of the energy eigenvalues and vice versa.

5.3 Partial wave expansion of the wavefunction

For distances greater than the potential radius but smaller than the period (the volume), the wavefunctions $\psi_{\vec{k}}(\vec{r})$ satisfy the free particle equation and can thus be written as

$$\psi_{\vec{k}}(\vec{r}) = \sum_{lm} c_{lm}(\vec{k}) R_l(r; q) Y_{lm}(\hat{r}_0) \tag{5.21}$$

where $c_{lm}(\vec{k})$ are coefficients to be determined by using eq. (5.20) and $Y_{lm}(\theta, \phi)$ are the spherical harmonics. The radial part $R_l(r, q)$ can be expressed as

$$R_l(r, q) = \cos\delta_l(q) \; j_l(qr) - \sin\delta_l(q) \; n_l(qr) \qquad r \geq R \tag{5.22}$$

where $\delta_l(q)$ are the two–particle infinite volume scattering phases, $j_l(qr)$ are the spherical Bessel functions and $n_l(qr)$ are the spherical Neumann functions. For later use it is useful to recall the Wronskian relations satisfied by the Bessel and Neumann functions

$$[j_l, R_l] = -\frac{\sin\delta_l(q)}{qr^2} \qquad [n_l, R_l] = -\frac{\cos\delta_l(q)}{qr^2} \tag{5.23}$$

where, as usual, the Wronskian of two functions is defined as

$$[f(x), g(x)] = f(x)\frac{\partial g(x)}{\partial x} - \frac{\partial f(x)}{\partial x}g(x) \tag{5.24}$$

5.4 Partial wave expansion of the greenian

In this section it is derived the partial wave expansion of the greenian. To this end, it is useful to recall the well known Neumann's expansion of the Green's function

$$-\frac{1}{4\pi}\frac{e^{iq\|\vec{r}-\vec{r}'\|}}{\|\vec{r}-\vec{r}'\|} = q\sum_{lm} j_l(qr)Y_{lm}(\hat{r})\left[n_l(qr') - ij_l(qr')\right]Y^*_{lm}(\hat{r}') \tag{5.25}$$

The previous relation is valid provided that $r < r'$ otherwise one has to exchange $\vec{r}$ and $\vec{r}'$ in the right–hand side. The Neumann expansion has to be inserted in the expression for the greenian that it is rewritten here below for the sake of clarity

$$g_{\vec{k}}(\vec{r}-\vec{r}_0;q) = -\frac{1}{4\pi}\sum_{\vec{n}\in\mathbf{Z}^3} e^{i\vec{k}\cdot\vec{n}L}\frac{e^{iq\|\vec{r}-\vec{r}_0-\vec{n}L\|}}{\|\vec{r}-\vec{r}_0-\vec{n}L\|} \tag{5.26}$$

It is convenient to separate out the term with $\vec{n} = \vec{0}$ from the remaining terms and to use the Neumann expansion by identifying $\vec{r}'$ with $\vec{r}_0$ in the first case and with $\vec{n}L$ in the remaining terms. In the end one obtains

$$g_{\vec{k}}(\vec{r}-\vec{r}_0;q) =$$

$$= -\frac{1}{4\pi}\frac{\cos\|\vec{r}-\vec{r}_0\|}{\|\vec{r}-\vec{r}_0\|} + \sum_{lm} D_{lm}(\vec{k},q)\; j_l(q\,\|\vec{r}-\vec{r}_0\|)\; Y_{lm}(\widehat{\vec{r}-\vec{r}_0}) \tag{5.27}$$

where the so called reduced structure coefficients are given by

$$D_{lm}(\vec{k},q) =$$

$$= \sum_{\vec{n}\in\mathbf{Z}^3-\{\vec{0}\}} e^{i\vec{k}\cdot\vec{n}L}Y_{lm}(\hat{n})\left[n_l(qnL) - ij_l(qnL)\right] - i\frac{q}{\sqrt{4\pi}}\delta_{l0}\delta_{m0} \tag{5.28}$$

There are many different, although equivalent from the mathematical point of view, ways to express the reduced structure coefficients some of which are more convenient than the previous relation for a numerical computation

of these quantities. In section 5.8 an expression suitable for the numerical calculation is derived.

It is useful to recall also the following well known identity that can be easily proved by using the expansion in spherical harmonics of a plane wave (see eq. (5.50))

$$i^{JK} j_J(qR) Y_{JK}(\hat{R}) =$$

$$= 4\pi \sum_{lm,l'm'} i^{l-l'} C_{JK;lm,l'm'} \; j_l(qr) \; j_{l'}(qr_0) \; Y_{lm}(\hat{r}) Y_{l'm'}(\hat{r}_0) \qquad (5.29)$$

where $R = \|\vec{r} - \vec{r}_0\|$. In the previous relation, use has been made of the Gaunt coefficients defined as follows

$$C_{JK;lm,l'm'} = \int d\Omega_{\vec{k}} Y_{JK}(\hat{k}) Y^*_{lm}(\hat{k}) Y_{l'm'}(\hat{k}) \qquad (5.30)$$

Inserting the identity of eq. (5.29) in the partial wave expansion of the greenian, as given in eq. (5.27), it is possible to rewrite this expansion in a form that will be used in the following section to write the quantization conditions in the same form obtained by Lüscher in ref. [73] in the case of periodic boundary conditions, namely

$$g_{\vec{k}} \quad (\vec{r} - \vec{r}_0; q) = q \sum_{lm} j_l(qr) \; Y_{lm}(\hat{r}) n_l(qr_0) \; Y^*_{lm}(\hat{r}_0)$$

$$+ \quad \sum_{lml'm'} j_l(qr) \; Y_{lm}(\hat{r}) \; \Gamma_{lm,l'm'}(\vec{k}, q) \; j_{l'}(qr_0) \; Y_{l'm'}(\hat{r}_0) \qquad (5.31)$$

where $r < r_0 < nL \neq 0$, and where the so called "structure coefficients" are defined as follows

$$\Gamma_{lm,l'm'}(\vec{k}, q) = 4\pi \; i^{l-l'} \sum_{JK} i^{-J} D_{JK}(\vec{k}, q) \; C_{JK;lm,l'm'} \qquad (5.32)$$

5.5 Generalized Lüscher quantization condition

The Lüscher quantization condition [73] can be now derived by substituting in eq. (5.20) the partial wave expansion of the wavefunctions given in eq. (5.21) and that of the greenian given in eq. (5.31). The result of this calculation is

$$q \sum_{lm} \quad j_l(qr) \; Y_{lm}(\hat{r}) \; [n_l, R_l] \; c_{lm} +$$

$$+ \sum_{lml'm'} j_l(qr) Y_{lm}(\hat{r}) \; \Gamma_{lm,l'm'} \; [j_{l'}, R_{l'}] \, c_{l'm'} = 0 \qquad (5.33)$$

By making use of the Wronskian relations of eq. (5.23), one gets

$$q \cos \delta_l(q)\ c_{lm} + \sum_{l'm'} \Gamma_{lm,l'm'}\ \sin \delta_{l'}(q) c_{l'm'} = 0 \tag{5.34}$$

The previous one is a linear homogeneous system of equations having as unknowns the coefficients c_{lm}. The following compatibility determinantal equation

$$\det \left[\Gamma_{lm,l'm'}(\vec{k}, q) + q \delta_{ll'} \delta_{mm'}\ \cot \delta_l(q) \right] = 0 \tag{5.35}$$

is the quantization conditions for the energy of the two–particle states on a finite volume. This equation can be used to calculate the scattering phases once the energy eigenvalues are know (for example from lattice calculations) or vice versa to calculate the spectrum of the two–particle state given the scattering phases (for example by the analytical knowledge of the interaction potential).

It is important to remember that the results obtained in this section are valid up to exponentially small corrections. In particular, eq. (5.35) can be used in quantum field theory only if the physical size of the finite volume is large enough to exclude the presence of residual polarization effects. These observations apply also to the results of the following sections.

5.6 Singular solutions

In the derivation of the quantization conditions it has been assumed that the solutions of the homogeneous time–independent Shrödinger equation

$$\left(\triangle + q^2 \right) \phi_{\vec{k}}(\vec{r}) = 0 \tag{5.36}$$

were absent. In order for $\phi_{\vec{k}}(\vec{r})$ to be different from zero the condition

$$q = \frac{\left\| \vec{\theta} + 2\pi \vec{n} \right\|}{L} \tag{5.37}$$

has to be satisfied for some integer vector $\vec{n}$ at fixed $\vec{\theta}$ together with a quantization condition that can be derived along the same lines that have been followed to obtain eq. (5.35). This can happen only on particular volumes L and/or for particular interactions. In the following these situations will not be discussed and the interested reader is referred to ref. [73] for a detailed discussion of the $\vec{\theta} = \vec{0}$ case.

5.7 Reducing to S–waves

From the phenomenological point of view the relevant situation is the one in which all the scattering phases can be assumed to vanish except the S–wave phase

$$\delta_l(q) = 0 \ , \qquad l > 0 \tag{5.38}$$

In this case the quantization conditions simplify enormously. Indeed one has

$$C_{00;00,00} = \frac{1}{(\sqrt{4\pi})^3} \int d\Omega_{\vec{k}} = \frac{1}{\sqrt{4\pi}} \tag{5.39}$$

that substituted in eq. (5.35) together with eq. (5.38) gives

$$\tan \delta_0(q) = -\frac{q}{\sqrt{4\pi}\ D_{00}(\vec{k}, q)} \tag{5.40}$$

or, equivalently,

$$\tan \delta_0(q) = -\frac{\sqrt{\pi}\ Q}{d_{00}(\theta, Q)} \tag{5.41}$$

As it is shown in eqs. (5.71), the right hand side of the previous equation is a dimensionless quantity that can be computed once and forever. It is useful to define

$$\tan \phi(\theta, Q) = \frac{\sqrt{\pi}\ Q}{d_{00}(\theta, Q)} \tag{5.42}$$

The definition of $\phi(\theta, Q)$ is completed by requiring the continuity of this function by respect the variable Q for each value of θ and by the condition

$$\phi(\theta, Q = 0) = 0 \ , \qquad 0 \leq \theta_i < 2\pi \tag{5.43}$$

5.8 Structure coefficients calculation

In this section a mathematical expression useful for the numerical calculation of the structure coefficients it is derived. From eq. (5.32) it comes out that the non trivial part of this problem consists in the calculation of the reduced structure coefficients. In the following an expression of the reduced structure coefficients, different from that already given in eq. (5.28), is derived in order to get a formula suitable for numerical evaluation. The starting point is again the greenian definition

$$g_{\vec{k}}(\vec{R}; q) = -\frac{1}{4\pi} \sum_{\vec{n} \in \mathbf{Z}^3} e^{i\vec{k}\cdot\vec{n}L} \frac{e^{iq\left\|\vec{R}-\vec{n}L\right\|}}{\left\|\vec{R}-\vec{n}L\right\|} \tag{5.44}$$

With the aim of expressing it in the Fourier space, the following well known identities are recalled

$$\frac{1}{(2\pi)^3}\int d\vec{x}\; e^{i(\vec{p}_1-\vec{p}_2)\cdot\vec{x}} = \delta(\vec{p}_1-\vec{p}_2) \tag{5.45}$$

$$\frac{1}{L^3}\sum_{\vec{p}_m} e^{i\vec{p}_m\cdot\vec{x}} = \sum_{\vec{n}\in\mathbf{Z}^3}\delta(\vec{x}-\vec{n}L)\;, \qquad \vec{p}_m = \frac{2\pi}{L}\vec{m} \tag{5.46}$$

$$\lim_{\varepsilon\to 0^+}\frac{1}{(2\pi)^3}\int d\vec{p}\;\frac{e^{i\vec{p}\cdot\vec{x}}}{p^2-(q^2+i\varepsilon)} = \frac{1}{(4\pi)}\frac{e^{iqx}}{x} \tag{5.47}$$

that allow one to write the following chain of equalities

$$\begin{aligned}
g_{\vec{k}}(\vec{R};q) &= -\frac{1}{(2\pi)^3}\lim_{\varepsilon\to 0^+}\sum_{\vec{n}\in\mathbf{Z}^3} e^{i\vec{k}\cdot\vec{n}L}\;\int d\vec{p}\;\frac{e^{i\vec{p}\cdot(\vec{R}-\vec{n}L)}}{p^2-(q^2+i\varepsilon)} \\
&= -\frac{1}{(2\pi)^3}\lim_{\varepsilon\to 0^+}\int d\vec{p}\;\frac{e^{i\vec{p}\cdot\vec{R}}}{p^2-(q^2+i\varepsilon)}\;\sum_{\vec{n}\in\mathbf{Z}^3} e^{i(\vec{k}-\vec{p})\cdot\vec{n}L} \\
&= -\lim_{\varepsilon\to 0^+}\int d\vec{p}\;\frac{e^{i\vec{p}\cdot\vec{R}}}{p^2-(q^2+i\varepsilon)}\;\frac{1}{(2\pi)^3}\int d\vec{x}\sum_{\vec{n}\in\mathbf{Z}^3}\delta(\vec{x}-\vec{n}L)e^{i(\vec{k}-\vec{p})\cdot\vec{x}} \\
&= -\lim_{\varepsilon\to 0^+}\frac{1}{L^3}\sum_{\vec{p}_m}\int d\vec{p}\;\frac{e^{i\vec{p}\cdot\vec{R}}}{p^2-(q^2+i\varepsilon)}\;\frac{1}{(2\pi)^3}\int d\vec{x}e^{i(\vec{k}+\vec{p}_m-\vec{p})\cdot\vec{x}} \\
&= -\lim_{\varepsilon\to 0^+}\frac{1}{L^3}\sum_{\vec{p}_m}\int d\vec{p}\;\frac{e^{i\vec{p}\cdot\vec{R}}}{p^2-(q^2+i\varepsilon)}\;\delta(\vec{k}+\vec{p}_m-\vec{p}) \\
&= -\frac{1}{L^3}\sum_{\vec{p}_m}\frac{e^{i(\vec{k}+\vec{p}_m)\cdot\vec{R}}}{(\vec{k}+\vec{p}_m)^2-q^2}
\end{aligned} \tag{5.48}$$

Thus, the greenian expression in the reciprocal space is given by

$$g_{\vec{k}}(\vec{R};q) = -\frac{1}{L^3}\sum_{\vec{q}_m}\frac{e^{i\vec{q}_m\cdot\vec{R}}}{\vec{q}_m^{\,2}-q^2}\;, \qquad \vec{q}_m = \vec{k}+\frac{2\pi}{L}\vec{m} \tag{5.49}$$

It is now possible to derive an expression for the KKR reduced structure coefficients in the reciprocal space. To this end one has to consider the following identity expressing a plane wave as an expansion in spherical harmonics

$$e^{i\vec{q}_m\cdot\vec{R}} = 4\pi\sum_{lm} i^l j_l(q_m R)\; Y^*_{lm}(\hat{q}_m)\; Y_{lm}(\hat{R}) \tag{5.50}$$

so that the greenian can be expanded as follows

$$g_{\vec{k}}(\vec{R};q) = \sum_{lm}\left(-\frac{4\pi\ i^l}{L^3}\sum_{\vec{q}_m}\frac{j_l(q_mR)}{j_l(qR)}\ \frac{Y^*_{lm}(\hat{q}_m)}{\vec{q}_m^2-q^2}\right) j_l(qR)\ Y_{lm}(\hat{R}) \tag{5.51}$$

In order to reproduce the same structure given in eq. (5.27) it should be noted that

$$\begin{aligned} g_{\vec{k}}(\vec{R};q) &= g_{\vec{k}}(\vec{R};q) - \frac{1}{4\pi}\frac{\cos(qR)}{R} + \frac{1}{4\pi}\frac{\cos(qR)}{R} \\ &= g_{\vec{k}}(\vec{R};q) - \frac{1}{4\pi}\frac{\cos(qR)}{R} + \frac{q}{4\pi}\cot(qR)\ \frac{\sin(qR)}{R} \\ &= g_{\vec{k}}(\vec{R};q) - \frac{1}{4\pi}\frac{\cos(qR)}{R} + \frac{q}{4\pi}\cot(qR)\ j_0(qR) \end{aligned} \tag{5.52}$$

By inserting the last identity in eq. (5.51) one obtains

$$g_{\vec{k}}(\vec{R};q) = -\frac{1}{4\pi}\frac{\cos(qR)}{R} + \sum_{lm} D_{lm}(\vec{k},q;R) j_l(qR)\ Y_{lm}(\hat{R}) \tag{5.53}$$

where

$$D_{lm}(\vec{k},q;R) = -\frac{4\pi i^l}{L^3}\sum_{\vec{q}_m}\frac{j_l(q_mR)}{j_l(qR)}\ \frac{Y^*_{lm}(\hat{q}_m)}{\vec{q}_m^2-q^2} + \frac{q}{\sqrt{4\pi}}\cot(qR)\ \delta_{l0}\ \delta_{m0} \tag{5.54}$$

This expression requires some comments. First it should be noted that

$$Y^*_{lm}(\hat{q}_m) = Y_{lm}(\hat{q}'_m) \qquad \vec{q}_m = (q^1_m, q^2_m, q^3_m) \qquad \vec{q}'_m = (q^1_m, -q^2_m, q^3_m) \tag{5.55}$$

so that, being the rest of the $\vec{q_m}$ dependence only through the modulus, one gets

$$D_{lm}(\vec{k},q;R) = -\frac{4\pi i^l}{L^3}\sum_{\vec{q}_m}\frac{j_l(q_mR)}{j_l(qR)}\ \frac{Y_{lm}(\hat{q}_m)}{\vec{q}_m^2-q^2} + \frac{q}{\sqrt{4\pi}}\cot(qR)\ \delta_{l0}\ \delta_{m0} \tag{5.56}$$

The second observation concerns the R–dependence of the reduced structure coefficients. Indeed, by comparing eq. (5.28) with the previous equation, it follows that this functional dependence is fictitious. This can be also understood by a careful analysis of eq. (5.53). The term

$$n_0(qR) = \frac{cos(qR)}{qR} \tag{5.57}$$

satisfies by its own the equation

$$\left(\triangle + q^2\right) n_0(qR) = -\frac{4\pi}{q}\delta(\vec{R}) \tag{5.58}$$

so that the remaining terms of the sum in eq. (5.53) must be regular solutions of the homogeneous Helmholtz's equation. A general solution of this kind can be expressed as a linear combination of the form

$$\hat{g}_{\vec{k}}(\vec{R};q) = \sum_{lm} D_{lm}(\vec{k},q) j_l(qR)\ Y_{lm}(\hat{R}) \tag{5.59}$$

where the $D_{lm}(\vec{k},q)$ do not depend upon R. Furthermore, the spherical Bessel functions near the origin behave as

$$j_l(qR) \stackrel{R\to 0}{\longrightarrow} (qR)^l \tag{5.60}$$

The fictitious R–dependence of the reduced structure coefficients as given in eq. (5.56) can be eliminated by taking the limit for R that goes to zero and by using the previous equation.

One has to consider eq. (5.56) as a properly regulated form of the KKR reduced structure coefficients and think to

$$D_{lm}(\vec{k},q) = -\frac{4\pi i^l}{q^l L^3} \sum_{\vec{q}_m} \frac{q_m^l\ Y_{lm}(\hat{q}_m)}{\vec{q}_m^2 - q^2} + \frac{\delta_{l0}\ \delta_{m0}}{\sqrt{4\pi}} \lim_{R\to 0} \frac{1}{R} \tag{5.61}$$

as a formal expression of the same objects.

5.8.1 Ewald's sums

In ref. [78] Kohn and Rostoker considered a method particularly convenient from the numerical point of view to evaluate the reduced structure coefficients. They pointed out that, following a prescription due to Ewald [79], the sum

$$S(x) = \sum_{\vec{q}_m} \frac{j_l(q_m R)\ Y_{lm}(\hat{q}_m)}{q_m^2 - q_2}\ e^{\frac{q^2 - q_m^2}{x}} \tag{5.62}$$

approximate the needed result $S(\infty)$ with an exponentially vanishing error. In ref. [80] the original observation of Kohn and Rostoker was further refined by Ham and Segall. They first recall two identities both due to Ewald; the first one is

$$\frac{e^{iq\left\|\vec{R}-\vec{n}L\right\|}}{\left\|\vec{R}-\vec{n}L\right\|} = \lim_{\varepsilon\to 0} \frac{2}{\sqrt{\pi}} \int_0^\infty dx\ e^{-(\vec{R}-\vec{n}L)^2 x^2 + \frac{q^2+i\varepsilon}{4x^2}} \tag{5.63}$$

The second identity can be proved as done before in order to express the greenian in the reciprocal space starting from its expression in the direct space and states

$$\sum_{\vec{n}\in\mathbf{Z}^3} e^{-(\vec{R}-\vec{n}L)^2x^2+i\vec{k}\cdot(\vec{n}L-\vec{R})} = \frac{(\sqrt{\pi})^3}{(Lx)^3}\sum_{\vec{p}_m} e^{i\vec{p}_m\cdot\vec{R}-\frac{q_m^2}{4x^2}} \qquad \vec{p}_m = \frac{2\pi}{L}\vec{m} \tag{5.64}$$

By starting again from the expression of the greenian in the direct space as given in eq. (5.44) one can write, by using the first identity (5.63),

$$g_{\vec{k}}(\vec{R};q) = -\frac{1}{2(\sqrt{\pi})^3}\lim_{\varepsilon\to 0}\sum_{\vec{n}\in\mathbf{Z}^3}\int_0^\infty dx\; e^{i\vec{k}\cdot\vec{n}L-(\vec{R}-\vec{n}L)^2x^2+\frac{q^2+i\varepsilon}{4x^2}} \tag{5.65}$$

The integration domain can be split in $\left[0,\frac{\sqrt{\eta}}{2}\right]$ and $\left[\frac{\sqrt{\eta}}{2},\infty\right]$, where η is a positive arbitrary constant. The greenian can be thus re-expressed as the sum of two terms

$$g_{\vec{k}}(\vec{R};q) = g^1_{\vec{k}}(\vec{R};q) + g^2_{\vec{k}}(\vec{R};q) \tag{5.66}$$

where, by performing the integration in the first term and by using the identity of eq. (5.64) in the second one, one obtains

$$\begin{aligned} g^1_{\vec{k}}(\vec{R};q) &= \frac{1}{L^3}\sum_{\vec{q}_m}\frac{e^{i\vec{q}_m\cdot\vec{R}+\frac{q^2-q_m^2}{\eta}}}{q^2-q_m^2} \\ g^2_{\vec{k}}(\vec{R};q) &= -\frac{1}{2(\sqrt{\pi})^3}\sum_{\vec{n}\in\mathbf{Z}^3}\int_{\frac{\sqrt{\eta}}{2}}^\infty dx\; e^{i\vec{k}\cdot\vec{n}L-(\vec{R}-\vec{n}L)^2x^2+\frac{q^2}{4x^2}} \end{aligned} \tag{5.67}$$

These series are absolutely convergent for any finite $\eta > 0$ and each term is an analytic function of q throughout the complex plane except for simple poles at $q^2 = q_m^2$. By expanding term-wise both $g^1_{\vec{k}}$ and $g^2_{\vec{k}}$ in spherical harmonics with respect to $\vec{R}$, taking the limit $R \to 0$, and comparing the result with the definition of the reduced structure coefficients, one gets

$$D_{lm}(\vec{k},q) = D^1_{lm}(\vec{k},q) + D^2_{lm}(\vec{k},q) + D^3_{lm}(\vec{k},q) \tag{5.68}$$

where

$$\begin{aligned} D^1_{lm}(\vec{k},q) &= \frac{4\pi}{L^3q^l}\; e^{\frac{q^2}{\eta}}\;\sum_{\vec{q}_m}\frac{q_m^l}{q^2-q_m^2}\; Y_{lm}(\hat{q}_m)\; e^{-\frac{q_m^2}{\eta}} \\ D^2_{lm}(\vec{k},q) &= -\frac{2^{l+1}L^li^l}{q^l\sqrt{\pi}}\sum_{\vec{n}\in\mathbf{Z}^3-\{\vec{0}\}} n^l\; e^{i\vec{k}\cdot\vec{n}L}\; Y_{lm}(\hat{n})\;\int_{\frac{\sqrt{\eta}}{2}}^\infty dx\; x^{2l}\; e^{-(x\vec{n}L)^2+\frac{q^2}{4x^2}} \\ D^3_{lm}(\vec{k},q) &= -\delta_{l0}\;\delta_{m0}\;\frac{\sqrt{\eta}}{2\pi}\sum_{s=0}^\infty\frac{q^{2s}}{\eta^s}\;\frac{1}{s!(2s-1)} \end{aligned} \tag{5.69}$$

In order to make more explicit the dependence of the reduced structure coefficients upon the volume it is convenient to define

$$\begin{aligned} d_{lm}(\theta, Q) &= L D_{lm}(\vec{k}, q) \\ &= d^1_{lm}(\theta, Q) + d^2_{lm}(\theta, Q) + d^3_{lm}(\theta, Q) \end{aligned} \tag{5.70}$$

and rewrite eqs. (5.69) as follows

$$\begin{aligned} d^1_{lm}(\theta, Q) &= \frac{i^l}{\pi Q^l}\, e^{\frac{Q^2}{\eta'}} \sum_{\vec{Q}_m} \frac{Q^l_m\, Y_{lm}(\hat{Q}_m)}{Q^2 - Q^2_m}\, e^{-\frac{Q^2_m}{\eta'}} \\ d^2_{lm}(\theta, Q) &= -\frac{4^{l+1} i^l \sqrt{\pi}}{Q^l} \sum_{\vec{n} \in \mathbf{Z}^3 - \{\vec{0}\}} (\pi n)^l e^{i\vec{\theta}\cdot\vec{n}} Y_{lm}(\hat{n}) \int_{\frac{\sqrt{\eta'}}{2}}^{\infty} dx x^{2l} e^{-(2\pi x \vec{n})^2 + \frac{Q^2}{4x^2}} \\ d^3_{lm}(\theta, Q) &= -\delta_{l0}\, \delta_{m0}\, \sqrt{\eta'} \sum_{s=0}^{\infty} \frac{Q^{2s}}{\eta'^s}\, \frac{1}{s!(2s-1)} \end{aligned} \tag{5.71}$$

where the following definitions have been also used

$$Q = \tfrac{Lq}{2\pi} \qquad\qquad Q_m = \left\| \vec{m} + \frac{\vec{\theta}}{2\pi} \right\| \tag{5.72}$$

$$\vec{k} = \tfrac{\vec{\theta}}{L} \qquad\qquad \eta' = \left(\frac{L}{2\pi}\right)^2 \eta \tag{5.73}$$

5.8.2 Incomplete Gamma Function

The computation of the reduced structure coefficients is complicated from the numerical point of view by the presence of an integral in the definition of $d^2_{lm}(\theta, Q)$. In order to simplify the numerical task it is useful to introduce the "incomplete gamma function":

$$\Gamma(\alpha, y) = \int_y^{\infty} dx\; x^{\alpha-1} e^{-x} \tag{5.74}$$

By using it, $d^2_{lm}(\theta, Q)$ can be rewritten in the form

$$\begin{aligned} d^2_{lm}(\theta, Q) &= -\frac{i^l \sqrt{\pi}}{Q^l} \times \\ &\times \sum_p \frac{Q^{2p}}{p!} \sum_{\vec{n} \in \mathbf{Z}^3 - \{\vec{0}\}} \frac{e^{i\vec{\theta}\cdot\vec{n}}}{(\pi n)^{l-2p+1}}\, Y_{lm}(\hat{n})\, \Gamma\left(l - p + \frac{1}{2}, (\pi n)^2 \eta'\right) \end{aligned} \tag{5.75}$$

The great advantage of this expression with respect to the one given in eq. (5.71) is that the incomplete gamma function can be computed numerically using a continued fraction representation:

$$\Gamma(\alpha, y) = \cfrac{e^{-y}\, y^{\alpha}}{x \;+\; \cfrac{1-\alpha}{1 + \cfrac{1}{x + \cfrac{2-\alpha}{1 + \cfrac{2}{x + \cfrac{3-\alpha}{1 + \cdots}}}}}} \tag{5.76}$$

5.9 Generalized Lellouch–Lüscher formula

In this section a generalization of the LL formula [70] is derived that connects the weak matrix element of the decay $K \to (\pi\pi)_I$ (being I the isospin of the state) calculated on a finite volume with the corresponding quantity in the infinite volume limit up to exponentially vanishing corrections. In the following it is considered a theory of spinless pions and kaons of masses such that the condition

$$2m_\pi < m_K < 4m_\pi \tag{5.77}$$

is satisfied. It is further assumed that the pions scatter purely elastically below the threshold for the production of four pions and that the kaon is stable in the absence of weak interactions. When the weak interactions are switched–on the kaon is allowed to decay into two pions and the transition amplitude is given by

$$T(K \mapsto \pi\pi) = A(\overline{q})\; e^{i\delta_0(\overline{q})} \tag{5.78}$$

where A is real, δ_0 is the S–wave scattering phase of the outgoing two–pion state and $\overline{q}$ is the pion momentum in the center-of-mass frame

$$\overline{q} = \frac{1}{2}\sqrt{m_K^2 - 4m_\pi^2} \tag{5.79}$$

In writing eq. (5.78) use has been made of the standard relativistic normalizations for the one–particle states together with the LSZ constraints on their phases

$$\langle 0|\varphi_\pi(x)|\pi(p)\rangle = \sqrt{Z_\pi}\; e^{-ipx}\;, \qquad \langle 0|\varphi_K(x)|K(p)\rangle = \sqrt{Z_K}\; e^{-ipx} \tag{5.80}$$

where φ_π and φ_K are the pion and kaon interpolating fields respectively.

The same theory is now considered on a finite volume of linear extension L. The finite volume one–particle states are normalized to unity and their

phases can be chosen arbitrarily. The transition amplitude on the finite volume is referred to as

$$A_L(\overline{q}) = \langle \pi\pi^L | H_W | K^L \rangle \tag{5.81}$$

where H_W is the weak interactions Hamiltonian. The generalized LL formula is given by

$$\|A(\overline{q})\|^2 = 8\pi \left\{ Q\frac{\partial\phi(\theta,Q)}{\partial Q} + q\frac{\partial\delta_0(q)}{\partial q} \right\}_{q=\overline{q}} \left(\frac{m_K}{\overline{q}}\right)^3 \|A_L(\overline{q})\|^2 \tag{5.82}$$

where $\phi(\theta, Q)$ has been defined previously in eq. (5.42). This powerful relation is valid under the same hypotheses that have been made in section 5.7 in order to derive eq. (5.41) plus two additional assumptions on the outgoing two–pion state. It has to be non degenerate and must have the same energy of the decaying kaon, in order for the resulting infinite volume decay amplitude to be computed at the physical point.

In the LL derivation one has $\theta = 0$ and the two–pions state of definite isospin happens to have an energy equal to the kaon mass only on a certain particular volume. In the present generalization of the LL formula the θ–dependence of $\phi(\theta, Q)$ can be used in order to obtain a sequence of volumes of growing sizes on which the calculations can be actually performed (see the section 5.10). Within this approach, by studying the residual functional dependence of the results upon the volume it will also be possible to answer to the questions raised in ref. [76] about the size of the finite volume corrections coming from the presence of the inelastic threshold.

In the particular case $\theta = 0$ the first seven energy levels of the outgoing two–pion states are non degenerate, as shown in ref. [73]. Care about the possible degeneracies of the outgoing states has to be taken also in the case $\theta \neq 0$ for the particular choices of the Bloch's angles used in the calculations.

A further generalization of eq. (5.82) with respect to the LL result can be achieved by following the arguments of ref. [76] where the LL formula is shown to be valid for all the states below the inelastic threshold and even outside the physical point ($q = \overline{q}$).

5.9.1 Derivation of eq.(5.82)

The generalized LL formula in eq. (5.82) is a direct consequence of the quantization condition. As already discussed, the kaon is assumed to be stable when weak interactions are switched off. Conversely, on the volumes where

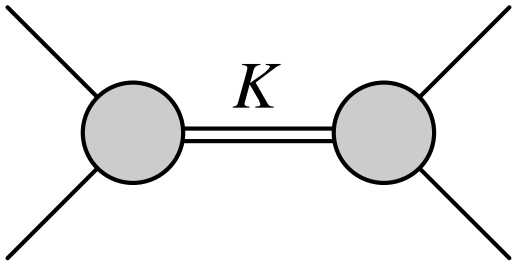

Figure 5.1: Kaon exchange contribution to the pion–pion scattering amplitude.

the energy of the scattering two–pion state equals the kaon mass, weak interactions are able to mix the two degenerate energy eigenstates $|K^L\rangle$ and $|\pi\pi^L\rangle$. The relevant part of H_W for this process is the strangeness changing. The energy of both the two–pion state and the kaon state is referred to as W. At the lowest order in the weak expansion W is given by

$$W = m_K = 2\sqrt{m_\pi^2 + q_\pi^2} \tag{5.83}$$

At first order, degenerate perturbation theory yields

$$W = m_K \pm \|A_L\| \qquad q = q_\pi \pm \underbrace{\frac{m_K}{4q_\pi}\|A_L\|}_{\Delta q} \tag{5.84}$$

These energy shifts can be calculated by including the presence of the kaon resonance in the scattering amplitude of the two pions. This contribution corrects the scattering phase as follows

$$\tilde{\delta}_0(q) = \delta_0(q) \mp \frac{q_\pi \|A\|^2}{32\pi m_K^2 \|A_L\|} \qquad (\text{mod } \pi) \tag{5.85}$$

The previous relation has been obtained by considering the graph of **Figure** [**5.1**] and by noting that the momenta flowing into the three–point vertexes are all on shell up to higher order corrections. As a consequence, the vertices's are proportional to the infinite volume kaon decay amplitude A and the kaon propagator is

$$\frac{iZ_K}{p_K^2 - m_k^2} = \pm\frac{iZ_K}{2m_K \|A_L\|} \tag{5.86}$$

The last step in the derivation consists in inserting $\tilde{\delta}_0$ into the quantization condition and in expanding all the terms in power series with respect to

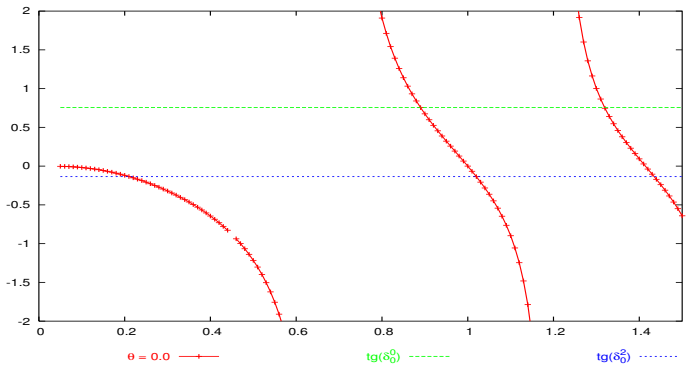

Figure 5.2: The red points represent $-\tan\phi(\theta, Q)$ as function of Q for $\theta = 0.0$. The different branches are the two–particle eigenvalues curves. The straight lines are the tangents of the scattering phases of two pions, having isospin $I = 0$ or $I = 2$, computed in chiral perturbation theory at the kaon mass.

the weak interactions

$$-\Delta q \left\{ \frac{\partial \delta_0(q)}{\partial q} \right\}_{q=q_\pi} + \frac{q_\pi \left\| A \right\|^2}{16\pi m_K^2 \left\| A_L \right\|} = \Delta Q \left\{ \frac{\partial \phi(\theta, Q)}{\partial Q} \right\}_{Q=Q_\pi} \tag{5.87}$$

This relation is in fact equivalent to eq. (5.82).

5.10 Spectrum of a two–pion state

In this section the spectrum of a two–pion system on finite volumes is studied assuming that the scattering phases for $l \geq 4$ are small in the elastic region (note that $\delta_l(q)$ is proportional to q^{2l+1} at low momenta). Under these hypotheses the energy quantization condition takes the simple form of eq. (5.41).

In fig. 5.2 the opposite of $\tan[\phi(\theta, Q)]$ for the particular choice $\theta = 0.0$ is shown. The points in which this function coincide with the function $\tan\delta_0(q)$ at fixed θ and L represent the two–particle eigenvalues on the given volume. Here below the following procedure will be carried on:

- the energy of the two particle state is fixed so that $q = \overline{q}$

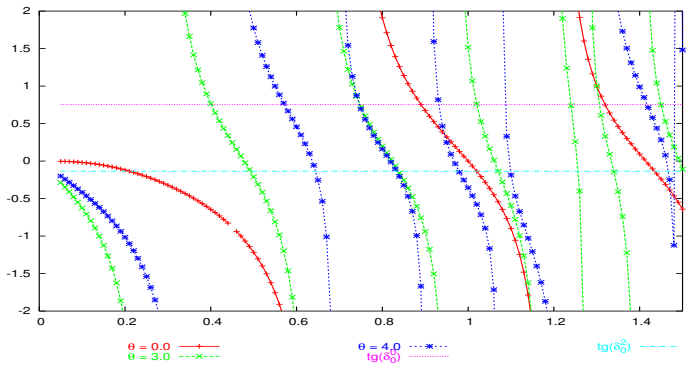

Figure 5.3: The points represent $-\tan\phi(\theta, Q)$ as functions of Q for different values of θ. The case $\theta = 2.5$ is not shown to help the eye. The straight lines are the tangents of two pions scattering phases, with isospin $I = 0$ or $I = 2$, computed in chiral perturbation theory at the kaon mass.

- the corresponding scattering phase $\delta_0(\overline{q})$ is computed by using the one–loop chiral perturbation theory results for these quantities [81, 82, 11, 83, 84]

- the solutions $\overline{Q}_n(\theta)$ of the condition

$$\tan\delta_0(\overline{q}) = -\tan\phi(\theta, \overline{Q}) \tag{5.88}$$

  are found

- the volume $\overline{L}_n(\theta)$ on which the n^{th} two–particle eigenvalue is equal to $\overline{q}$ is computed according to

$$\overline{L}_n(\theta) = 2\pi\frac{\overline{Q}_n(\theta)}{\overline{q}} \tag{5.89}$$

Following these steps it is possible to find for each value of θ the finite volumes on which a given energy level of a two–pion state equals the kaon mass. In ref. [70] the authors have not considered the possibility of having $\theta \neq 0$ and their analysis, that is reproduced in **Figure** [**5.2**], gives the following results

$$\begin{array}{lll} I = 0 & \overline{Q}_1(0) = 0.89 & \overline{L}_1(0) = 5.34 \text{ fm} \\ I = 2 & \overline{Q}_1(0) = 1.02 & \overline{L}_1(0) = 6.09 \text{ fm} \end{array} \tag{5.90}$$

θ	I	$\overline{Q}_1$	L_1
0.0	0	0.890	5.34
0.0	2	1.015	6.09
2.5	0	0.295	1.78
2.5	2	0.415	2.49
3.0	0	0.400	2.40
3.0	2	0.490	2.94
4.0	0	0.569	3.41
4.0	2	0.645	3.86

Table 5.1: Volumes on which the energy of the first eigenvalue two–pion state equals the K–meson mass. I is the isospin of the state.

In **Figure** [**5.3**] the same analysis is repeated for other allowed values of θ. As can be seen a careful choice of the "Bloch angle" shifts the position of the first eigenvalue curves at lower values of $\overline{Q}$ and consequently, being $\overline{q}$ fixed, at lower values of the physical volume. The resulting volumes corresponding to some particular choices of θ are given in **Table** [**5.1**].

5.11 Generalized LL–formula vs. lattice simulations

The generalization of the Lellouch–Lüscher formula derived in section 5.9 has been obtained under the hypothesis of a theory including in its spectrum pions and kaons. In particular the pions have been asked to satisfy θ–boundary conditions. A further assumption, implicitly made in the derivation, is that the isospin was a symmetry of the theory. Unfortunately, it is not possible to satisfy all these hypotheses in lattice simulations because of two different reasons.

The first problem has been already discussed in the previous chapter, precisely in section 4.6, and concerns the impossibility of choosing different boundary conditions for up and down quarks in unquenched simulations when the Wilson formulation is used. This does not allow the charged pions to

satisfy θ–BC with θ different from zero. The problem is better explained by considering, for example, the decay of a neutral kaon in charged pions. In order to have the kaon at rest, since the anti–quarks have a θ–angle opposite to that of the corresponding quarks, one has to chose strange and down quarks boundary conditions so that

$$\vec{\theta}_s = \vec{\theta}_d \tag{5.91}$$

At the same time, the positive charged pion interpolating field will have an overall θ–angle given by

$$\vec{\theta}_{\pi^+} = \vec{\theta}_u - \vec{\theta}_d \tag{5.92}$$

while for the negative pion one has $\vec{\theta}_{\pi^-} = -\vec{\theta}_{\pi^+}$, so that the total momentum of the two–pion system is zero. There is no problem to fulfill these conditions in the quenched theory but, when one considers the full theory, some technical complications arise. Indeed current simulation algorithms require the product of the quark determinants (that depend upon θ) to be non negative and, when Wilson fermions are considered, this implies that

$$\vec{\theta}_u = \vec{\theta}_d \tag{5.93}$$

i.e. a vanishing θ–angle for the interpolating fields of the charged pions. Nevertheless this complication does not arise when Ginsparg–Wilson fermions are considered because in this case the determinant of each quark is non negative.

The second problem has been pointed out in ref. [17] and concerns the breaking of the isospin symmetry by the choice of different θ–angles for the two light quarks. It is useful to write the action of the theory in the following compact form

$$S_F[\overline{\psi}, \psi, U] = \int d^4x \overline{\psi}(x) \left[\not{D} + m \right] \psi(x) \tag{5.94}$$

where

$$\psi(x) = \begin{pmatrix} u(x) \\ d(x) \end{pmatrix} \tag{5.95}$$

and the boundary conditions satisfied by $\psi(x)$ are

$$\psi(x + \vec{n}L) = \begin{pmatrix} e^{i\vec{\theta_u}\vec{n}} & 0 \\ 0 & e^{i\vec{\theta_d}\vec{n}} \end{pmatrix} \psi(x) \tag{5.96}$$

The isospin problem is better realized by making the following transformation on the fields

$$q(x) = \begin{pmatrix} e^{-i\frac{\theta_u x}{L}} & 0 \\ 0 & e^{-i\frac{\theta_d x}{L}} \end{pmatrix} \psi(x) \tag{5.97}$$

As a consequence of this transformation, the two component field $q(x)$ satisfy periodic boundary conditions but the action take the form

$$S_F[\overline{q},q,U]=\int d^4x\overline{q}(x)\left[\not{D}-i\frac{\not{\theta}_u+\not{\theta}_d}{2L}-i\frac{\not{\theta}_u-\not{\theta}_d}{2L}\tau_3+m\right]q(x) \qquad (5.98)$$

In this form it is easy to realize that the isospin rotations generated by τ_3 are symmetries of the theory while those generated by τ_1 or τ_2 do not commute with the Lagrangian anymore.

Since isospin is broken it is no more possible to distinguish between neutral two–pion states with $I=2$ or $I=0$ and, consequently, it is not possible to resolve the $\Delta I=1/2$ puzzle, even if Ginsparg–Wilson fermions are used in lattice simulations. Nevertheless, isospin is broken only by boundary terms and the the eigenvalues of τ_3 are still good quantum numbers to label the energy eigenstates of the theory. Actually[1], the isospin problem can be overcome by repeating the calculations that led to the derivation of the quantization condition and the generalized LL formula with the inclusion of different pion species (π^+,π^- and π^0) satisfying different θ–boundary conditions. The new calculation is underway.

[1]The author gratefully acknowledges many useful discussions with M. Lüscher on this point

Conclusions

In all the problems discussed in this thesis it has been shown that relevant phenomenological informations can be extracted by a clever use of finite volume calculations (recursion, boundary conditions, etc.).

In the first part it has been introduced a finite volume recursion technique, the step scaling method, devised in order to study systems characterized by two largely separated energy scales. The method has been applied in chapter 2 to perform the first quenched calculation of the b–quark mass in the continuum limit of lattice regularization. The step scaling method has been also applied in chapter 3 to calculate the decay constant of the B_s meson in the continuum limit of quenched lattice QCD. Although these quantities had already been calculated in previous works, the results discussed in this thesis are more accurate than the past ones because the step scaling method introduces much less systematics with respect to other methods commonly used to handle the same problems. For example, in the SSM calculation of the b–quark mass one need to use extrapolations only to connect numerical data with the continuum results; in other methods, on the contrary, one has to resort to effective theories or to extrapolations hardly controllable from the numerical point of view. In the SSM calculation of the heavy–light decay constants extrapolations are needed again to obtain results in the continuum but also to obtain the step scaling functions at the high energy reference scale. The extrapolated step scaling functions differ from the calculated ones by an amount of the order of $2-3\%$ while in a typical HQET calculation of the same quantities, the extrapolated results differ from the calculated ones of the order of 20%. At the present, the step scaling method has been used to calculate observables related to one–particle states. This is the case of the meson masses as well as of the decay constants. The method is expected to retain its validity also in the case of more complicate heavy–light observables. It can be used for example to calculate the Isgur–Wise function or even light–light form factors at high momentum transfer. Finally, the step scaling method retains its validity also in the case of simulations of the full theory

(unquenching). In this case it would be possible to calculate, among other things, the decay constant of the B meson since the chiral extrapolations are not affected by the presence of unphysical chiral logs.

In part II of this thesis it has been argued that a particular choice of boundary conditions, the so called θ–BC, helps in overcoming the problem represented by the 3–momenta quantization rule on finite volumes. To this end, in chapter 4 it has been shown by means of a simple numerical test that it is possible to handle "continuous" momentum transfers in finite volume lattice simulations by using different θ–BC for the different particles involved in the process under consideration.

In chapter 5, θ–boundary conditions have been used to study finite volume two–particle scattering states. The energy of a scattering state on a finite volume is subject to a quantization rule. In this thesis the quantization condition has been derived in the case of particles satisfying θ–BC. In chapter 5 it has been also derived a generalization of the so called Lellouch–Lüscher formula to the θ–BC case. This formula maps the non leptonic matrix element for the decay of a kaon into two pions with the corresponding quantity in the infinite volume and is valid, up to corrections exponentially vanishing with the volume, in a $\lambda\phi^4$ theory describing the interactions between kaons and pions. The usefulness of the formula in the case of QCD lattice simulations is hardly limited by the fact that it is not possible to enforce θ–BC on the pions interpolating fields without breaking isospin at the quark level. Further work is needed to overcome these difficulties but a solution can be found by repeating the calculations along the same lines discussed in the present work.

Acknowledgments

It is a great pleasure for me to thank all the peoples I have worked with during the three years of my Ph.D. course: G.M. de Divitiis, M. Guagnelli and F. Palombi. I have learned too much things about physics by working with them too be able in few words to express all my gratitude.

My kind gratitude goes also to M. Lüscher. The results discussed in Part II of this thesis would have not been obtained without his invaluable suggestions.

In particular, I am very happy for having the opportunity to thank the most creative thinker I ever encountered in my life, Roberto Petronzio. I am always very impressed by his peculiar way of reasoning. I am glad to share with him his views about physics, about life.

Bibliography

[1] M. Guagnelli et al., Phys. Lett. B546 (2002) 237, hep-lat/0206023.

[2] G.M. de Divitiis et al., Nucl. Phys. B675 (2003) 309, hep-lat/0305018.

[3] G.M. de Divitiis et al., Nucl. Phys. B672 (2003) 372, hep-lat/0307005.

[4] G.M. de Divitiis, R. Petronzio and N. Tantalo, Phys. Lett. B595 (2004) 408, hep-lat/0405002.

[5] V. Gimenez et al., JHEP 03 (2000) 018, hep-lat/0002007.

[6] HPQCD, A. Gray et al., (2002), hep-lat/0209022.

[7] C.W. Bauer et al., (2002), hep-ph/0210027.

[8] M. Battaglia et al., (2002), hep-ph/0210319.

[9] R. Sommer, (2002), hep-lat/0209162.

[10] J. Heitger, M. Kurth and R. Sommer, (2003), hep-lat/0302019.

[11] J. Gasser and H. Leutwyler, Nucl. Phys. B250 (1985) 465.

[12] H. Leutwyler, (2000), hep-ph/0008124.

[13] A. Pich, Rept. Prog. Phys. 58 (1995) 563, hep-ph/9502366.

[14] G. Ecker, (2000), hep-ph/0011026.

[15] U.G. Meissner, Rept. Prog. Phys. 56 (1993) 903, hep-ph/9302247.

[16] G. Colangelo and G. Isidori, (2000), hep-ph/0101264.

[17] C.T. Sachrajda and G. Villadoro, (2004), hep-lat/0411033.

[18] M. Neubert, Phys. Rept. 245 (1994) 259, hep-ph/9306320.

[19] A.V. Manohar and M.B. Wise, Camb. Monogr. Part. Phys. Nucl. Phys. Cosmol. 10 (2000) 1.

[20] G.M. de Divitiis et al., Work in progress.

[21] A. Stocchi, (2002), hep-ph/0211245.

[22] M. Ciuchini et al., JHEP 07 (2001) 013, hep-ph/0012308.

[23] A. Hocker et al., Eur. Phys. J. C21 (2001) 225, hep-ph/0104062.

[24] A.J. Buras, F. Parodi and A. Stocchi, (2002), hep-ph/0207101.

[25] ALPHA, J. Rolf and S. Sint, JHEP 12 (2002) 007, hep-ph/0209255.

[26] Particle Data Group, K. Hagiwara et al., Phys. Rev. D66 (2002) 010001.

[27] M. Luscher et al., Nucl. Phys. B384 (1992) 168, hep-lat/9207009.

[28] S. Sint, Nucl. Phys. B421 (1994) 135, hep-lat/9312079.

[29] M. Luscher et al., Nucl. Phys. B413 (1994) 481, hep-lat/9309005.

[30] M. Luscher and P. Weisz, Nucl. Phys. B479 (1996) 429, hep-lat/9606016.

[31] M. Luscher et al., Nucl. Phys. B478 (1996) 365, hep-lat/9605038.

[32] M. Luscher et al., Nucl. Phys. B491 (1997) 323, hep-lat/9609035.

[33] M. Guagnelli and R. Sommer, Nucl. Phys. Proc. Suppl. 63 (1998) 886, hep-lat/9709088.

[34] S. Sint and P. Weisz, Nucl. Phys. B502 (1997) 251, hep-lat/9704001.

[35] S. Capitani et al., Nucl. Phys. Proc. Suppl. 63 (1998) 153, hep-lat/9709125.

[36] G.M. de Divitiis and R. Petronzio, Phys. Lett. B419 (1998) 311, hep-lat/9710071.

[37] ALPHA, M. Guagnelli et al., Nucl. Phys. B595 (2001) 44, hep-lat/0009021.

[38] R. Sommer, Nucl. Phys. B411 (1994) 839, hep-lat/9310022.

[39] ALPHA, M. Guagnelli, R. Sommer and H. Wittig, Nucl. Phys. B535 (1998) 389, hep-lat/9806005.

[40] S. Necco and R. Sommer, Nucl. Phys. B622 (2002) 328, hep-lat/0108008.

[41] M. Guagnelli, R. Petronzio and N. Tantalo, Phys. Lett. B548 (2002) 58, hep-lat/0209112.

[42] ALPHA, J. Garden et al., Nucl. Phys. B571 (2000) 237, hep-lat/9906013.

[43] T. van Ritbergen, J.A.M. Vermaseren and S.A. Larin, Phys. Lett. B400 (1997) 379, hep-ph/9701390.

[44] J.A.M. Vermaseren, S.A. Larin and T. van Ritbergen, Phys. Lett. B405 (1997) 327, hep-ph/9703284.

[45] K.G. Chetyrkin, Phys. Lett. B404 (1997) 161, hep-ph/9703278.

[46] M. Luscher et al., Nucl. Phys. B491 (1997) 344, hep-lat/9611015.

[47] N. Yamada, (2002), hep-lat/0210035.

[48] D. Becirevic, (2002), hep-ph/0211340.

[49] C.W. Bernard and M.F.L. Golterman, Phys. Rev. D46 (1992) 853, hep-lat/9204007.

[50] S.R. Sharpe, Phys. Rev. D46 (1992) 3146, hep-lat/9205020.

[51] M.J. Booth, Phys. Rev. D51 (1995) 2338, hep-ph/9411433.

[52] S.R. Sharpe and Y. Zhang, Phys. Rev. D53 (1996) 5125, hep-lat/9510037.

[53] M. Luscher, (2000), hep-th/0102028.

[54] D.J. Gross and Y. Kitazawa, Nucl. Phys. B206 (1982) 440.

[55] A. Roberge and N. Weiss, Nucl. Phys. B275 (1986) 734.

[56] K. Jansen et al., Phys. Lett. B372 (1996) 275, hep-lat/9512009.

[57] A. Bucarelli et al., Nucl. Phys. B552 (1999) 379, hep-lat/9808005.

[58] J. Kiskis, R. Narayanan and H. Neuberger, Phys. Rev. D66 (2002) 025019, hep-lat/0203005.

[59] Zeuthen-Rome / ZeRo, M. Guagnelli et al., (2003), hep-lat/0303012.

[60] J. Kiskis, R. Narayanan and H. Neuberger, Phys. Lett. B574 (2003) 65, hep-lat/0308033.

[61] P.F. Bedaque, (2004), nucl-th/0402051.

[62] S. Duane et al., Phys. Lett. B195 (1987) 216.

[63] P. de Forcrand and T. Takaishi, Nucl. Phys. Proc. Suppl. 53 (1997) 968, hep-lat/9608093.

[64] M.J. Peardon, (2000), hep-lat/0011080.

[65] M. Hasenbusch, Phys. Lett. B519 (2001) 177, hep-lat/0107019.

[66] M. Hasenbusch and K. Jansen, Nucl. Phys. B659 (2003) 299, hep-lat/0211042.

[67] ALPHA, M. Della Morte et al., Comput. Phys. Commun. 156 (2003) 62, hep-lat/0307008.

[68] M. Luscher, (2004), hep-lat/0409106.

[69] L. Giusti, Nucl. Phys. Proc. Suppl. 119 (2003) 149, hep-lat/0211009.

[70] L. Lellouch and M. Luscher, Commun. Math. Phys. 219 (2001) 31, hep-lat/0003023.

[71] M. Luscher, Commun. Math. Phys. 104 (1986) 177.

[72] M. Luscher, Commun. Math. Phys. 105 (1986) 153.

[73] M. Luscher, Nucl. Phys. B354 (1991) 531.

[74] M. Luscher, Nucl. Phys. B364 (1991) 237.

[75] M. Luscher and U. Wolff, Nucl. Phys. B339 (1990) 222.

[76] C.J.D. Lin et al., Nucl. Phys. B619 (2001) 467, hep-lat/0104006.

[77] J. Korringa, Physica (Utrecht) 13 (1947) 392.

[78] W. Kohn and N. Rostoker, Phys. Rev. 94 (1954) 1111.

[79] P. Ewald, Ann. Physik. 64 (1921) 253.

[80] F.S. Ham and B. Segall, Phys. Rev. 124 (1961) 1786.

[81] J. Gasser and H. Leutwyler, Phys. Lett. B125 (1983) 325.

[82] J. Gasser and H. Leutwyler, Ann. Phys. 158 (1984) 142.

[83] J. Gasser and U.G. Meissner, Phys. Lett. B258 (1991) 219.

[84] M. Knecht et al., Nucl. Phys. B457 (1995) 513, hep-ph/9507319.